MASTER THESIS

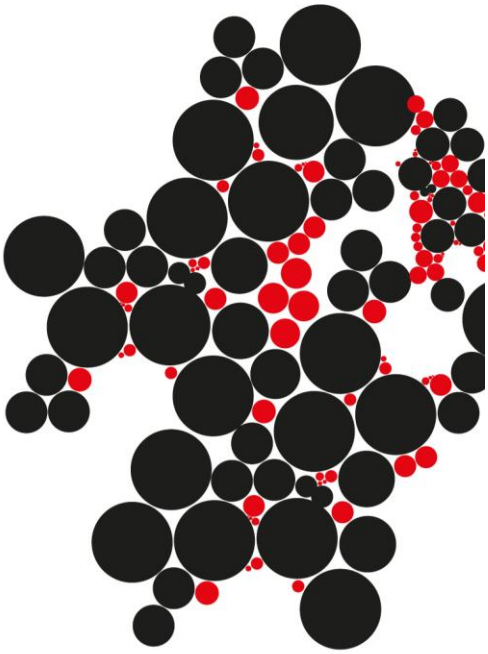

ACTIVE NOISE REDUCTION IN DOUBLE-PANEL STRUCTURES: DECENTRALIZED ADAPTIVE FEEDFORWARD CONTROL

Jurgen Kalverboer

DEPARTMENT OF ELECTRICAL ENGINEERING
SIGNALS AND SYSTEMS GROUP (SAS)

EXAMINATION COMMITTEE
Dr.ir. A.P. Berkhoff
Jen-Hsuan Ho, MSc.
Prof.dr.ir. C.H. Slump
Ir. E.R. Kuipers

DOCUMENT NUMBER
SAS – 2012-012

UNIVERSITY OF TWENTE.

06-07-2012

Abstract

In this thesis an adaptive harmonic decentralized feedforward controller is implemented on an experimental setup. The experimental setup consists of a double-panel structure which is mounted on top of an acrylic box with thick walls. In this box a speaker is installed which can produce disturbance signals. On each panel of the double-panel structure five actuator sensor pairs are installed which are controlled and observed by their own decentralized controller .The goal of this thesis is to minimize the sound transmission of the double-panel structure. The damping of the panel is increased by adding a low-authority feedback controller. The disturbance signal will contain only a few deterministic frequency components. Each frequency component is processed independently, by the harmonic decentralized controllers on the panels.

The stability and convergence rate of decentralized feedforward control is analysed. In simulations it is demonstrated that a decentralized controller can reduce the noise transmission of the structure. There are multiple feedforward control configurations possible, for example, one strategy might only control the incident panel. The most noise reduction is obtained by controlling only the radiant panel. This configuration can reduce the sound pressure level above the panel by 10 to 20 dB for frequencies below 250 Hz. Above this frequency almost no reduction of the disturbance signal is possible.

The addition of feedback control improves the robustness of the system. It reduces the cross-coupling between the decentralized controllers. There are also multiple feedback control configurations possible. The combination of feedback pressure speakers in the cavity and decentralized feedforward control of the radiant panel reduces the disturbance signal the most in the simulations. In practise this configuration could not be tested, because the pressure speaker feedback controller has not yet been realized.

For optimal control of the double-panel structure the transfer functions between all actuators and sensors in the system must be known. Therefore, a system identification technique is developed. This technique uses the computational components available in the decentralized controllers. The communication with a centralized controller is minimized.

Contents

1 Introduction 3
1.1 Aircraft noise 3
1.2 Active noise control 4
1.3 Research objective 7
1.4 Thesis outline 8
2 Acoustics 9
2.1 Propagation of waves 9
2.2 Acoustic quantities 10
2.3 Sound radiation from structures 11
3 Adaptive Harmonic Decentralized Feedforward Controller 13
3.1 Harmonic feedforward controller 13
3.2 Adaptive harmonic feedforward controller 15
3.3 Control effort weighting 16
3.4 Decentralized controller 17
3.5 Gersgorin's Theorem 18
3.6 Principal component analysis 21
3.7 Phasor arithmetic 24
3.8 Error signal detection 25
4 System identification 27
4.1 Possible implementations 28
4.2 Excitation signals 28
4.3 Conclusion 31
5 Simulations 31
5.1 Control effort weighting 32
5.2 Adaptive decentralized Harmonic controller 35
6 Implementation 40
6.1 Stepped sine system identification 41
6.2 System identification parallel 42
6.3 Decentralized feedforward controller 43
7 Experiments 45
7.1 The experimental setup 45
7.2 Measurement system 46
7.3 Frequency response analysis 48
7.4 Transient state inspection 49

7.5 System identification 51
7.6 Offline analysis 53
7.7 Adaptive harmonic feedforward controller 55
7.8 Varying disturbance frequency 59
8 Conclusion and recommendations 60
8.1 Conclusion 61
8.2 Recommendations 62
9 Bibliography 64

1 Introduction

This introduction chapter starts with a literature survey of aircraft noise and active noise control. After this survey the research questions are formulated and the ultimate goal of this thesis is presented. This introduction concludes with an outline of the content of this thesis.

1.1 Aircraft noise

Aircraft noise is a major problem for residents near airports. However, also people inside an aircraft get disturbed by the noise the engines produce. The interior noise in an aircraft is mainly produced by two external sources, the fuselage boundary layer and the aircraft propulsion system. In Figure 1 these disturbances are illustrated. The boundary layer noise is generated by movement of the fuselage wall. This wall moves through the outside pressure fluctuations produced by wind and turbulence. This noise is difficult to reduce because it has a stochastic broadband disturbance, for which no time advanced reference signal is available.

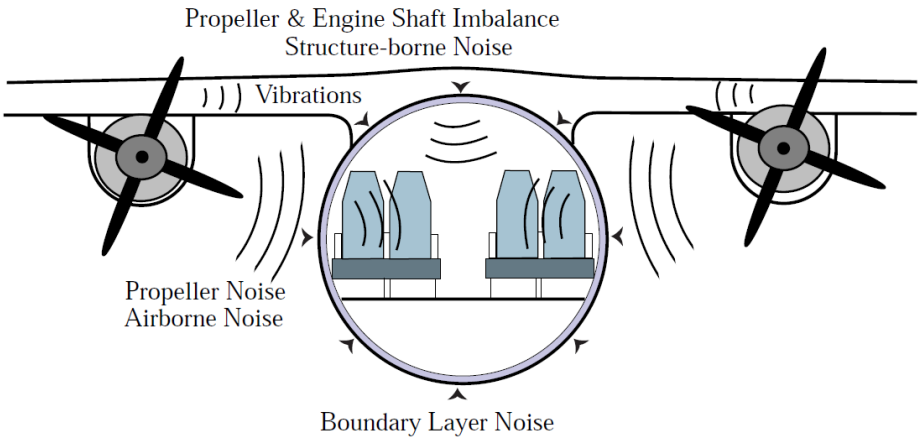

Figure 1 Aircraft noise.

Currently most passenger aircrafts are equipped with jet engines which produce broadband noise. An advantage of jet engines is that they produce less noise at the lower frequencies than propeller propulsed aircrafts [1]. The noise generated by a propeller engine contains a few specific frequency components which are equal to the blade passage frequency (BPF) of the propeller and some of its higher harmonics [2]. In Figure 2 the power spectrum in the cabin of a propeller propulsed aircraft is shown.

Recent developments make propeller engines more fuel efficient than yet engines, because of this reason some mayor aerospace corporations want to equip their commercial airplanes with propeller engines. The rotation frequency of the propellers can be measured, and thus the disturbance signal they generate can be predicted.

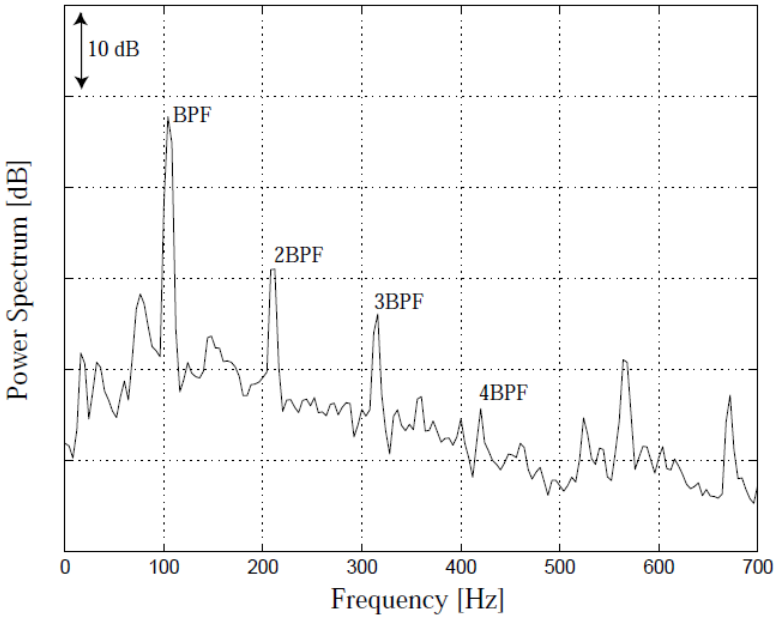

Figure 2 Noise in the cabin of a propeller propulsed aircraft.

1.2 Active noise control

Passive control is the traditional method to reduce the sound pressure at a given location. This technique uses an object that will absorb the radiated power of the disturbance source. The wavelength of the noise source must be small compared to the dimensions of the power absorbing object to well function. So this type of noise control works best for high frequencies [3] [4]. For lower frequencies you need larger damping objects which have a larger mass. For fuel efficiency, airplanes have to be as lightweight as possible so this is an unwanted feature. There are also more advanced passive control techniques such as for example a Helmholtz resonator. A Helmholtz resonator can increase the acoustical damping level inside a cavity between two plates. Simulations have shown that this can result in an overall improvement of 8dB in the 50-150 Hz range [5].

The other newer method, active control, uses secondary sources which generate a field that will interfere with the field produced by the primary noise source. This field will cancel the primary field, resulting in a reduced sound pressure. If the secondary sources are placed within half a wavelength of the disturbance signal of the primary source in all directions the field will be cancelled by a considerable amount [6] [7]. Although in most applications a similar setup is not possible, still active noise control performs well, especially at low frequencies. The main advantage compared to passive control is that no heavy objects are required for the reduction in sound pressure.

ANC and ASAC

There are two active noise control methods, active noise control (ANC) and active noise and vibration control (ANVC), these methods can be used to control tonal noise disturbances in relative small enclosures [8]. The former method uses loudspeakers to cancel the disturbance source. Every speaker will only cancel the disturbance signal at a few points in space. So all these secondary speakers need to cooperate, which will result in a complex 3D model. The global sound pressure in a space can be estimated by using multiple error sensors, each positioned at a different location [8]. The performance of this control system can be quantified by measuring the average attenuation at all measurement sensors.

The ASAC method uses a vibrating plate to reduce the transmission of the disturbance source. On this plate actuators and sensors are integrated so that the vibration of the plate can be observed and controlled. By controlling the vibration of the plate the sound transmission through the plate can be reduced. This simplifies the control problem to a two dimensional problem, because only the surface of the plate needs to be controlled.

A vibrating panel radiates with a set of structural modes. Each mode has a sinusoidal component in both directions of the panel. The spatial frequencies of these modes are dependent on the dimensions of the panel. The radiation of sound of each mode is dependent on the amplitudes of all modes. For some vibration patterns the air in front of the panel can transfer from one side of the panel to the other. Such patterns will not radiate much sound, only vibration patterns that have a net volumetric component will produce a significant amount of sound [9]. The far-field sound radiation of a plate can thus be estimated by measuring the net volume velocity of the panel. The lower modes of the panel are the most efficient radiation modes [10] [11] [12].

Double panel structures can be used as noise insulators. In general they perform better than single panel structures. However, at low frequencies around the mass-air-mass resonance (double structures resonance) they perform worse than single panel structures. In the past years many techniques have been developed to solve this problem. These techniques can be classified in active control and passive control [5].

Tonal and broadband disturbances

The tonal disturbance signal produced by the propeller engines contains only disturbances at a few harmonics. For these different harmonics a separate control filter, a harmonic controller, can be implemented. A harmonic controller measures only the error of that specific harmonic. It is advised to use an adaptive control filter for deterministic tonal disturbances. Because, the transmission from the disturbance source to the error sensor may change due to environmental changes [7]. An adaptive control filter can react on the phase and the magnitude variations of the disturbance signal so that the error is minimalized.

If the disturbance source produces a broadband disturbance signal the above mentioned method is not suitable. The separate control filters will interfere with each other, and abrupt phase changes cannot be realised. In this case only a single filter for the entire spectrum can be used. This filter must be causal, which will limit its performance [7]. Implementing the controller in the frequency domain will reduce the computational complexity. The convergence speed of the adaptive algorithm is similar to the time-domain solution.

Adaptive feedforward control

The simplest adaptive algorithm is the steepest descent algorithm. This algorithm is implemented in the frequency domain, it adjusts the in-phase and quadrature components of the single tone signal fed to the secondary sources [13]. There are other adaptive methods available such as Newton's algorithm or recursive least squares. These algorithms may have better convergence behaviour under certain circumstances. However, these methods have higher computational requirements [14] [7].

An adaptive feedforward controller usually formulates a cost function [7]. At each iteration the algorithm tries to minimise the cost. Therefore, it uses the Hessian matrix, this is the second derivate

of the cost function with respect to the control effort. Every eigenvalue of the Hessian matrix is related to a mode of the system. Every mode has its own power and convergence rate. The speed of convergence of a mode is determined by the magnitude of the eigenvalue. Slow modes require an excessive high control effort. To limit the required effort a control effort weighting function can be added to the cost function, which will increase the eigenvalues of the system. Modes for which the eigenvalues are much smaller than the effort weighting parameter will not converge. Their contribution in the error signals of these modes will not be removed [13] [6].

The adaptation rate of a steepest descent adaptive filter is dependent on the convergence coefficient of the filter. If the convergence coefficient value is too small, the algorithm will stop before the minimum error is reached. On the other hand, if this value is chosen to large the system will become unstable. For SISO systems the convergence coefficient is limited by the time delays in the cancellation paths of the secondary sources (23) [6]. For MIMO systems this is limited by the eigenvalues of the modes [13]. Faster adaptation does not result in better system performance, it usually decreases it. During fast adaptation unexcited system modes may be triggered, and this can lead to a performance decrease. A large sensor noise can also excite these unreferenced signal modes [15].

Model errors in adaptive controllers may lead to unstable systems or increased error signals [16]. By adding a bounded uncertainty region to the complex plant response optimal control can be obtained without making the system unstable [17].

Centralized and decentralized control

In comparison to centralized control, decentralized control is more scalable, however since each controller is designed based only on local sensor information (rather than all available sensor data), the performance is usually not as good as with a centralized control system.

For the communication between the centralized controller and the error sensors is a great deal of wiring required (see Figure 3). Not all applications will have the required space for this wiring. Another disadvantage of a centralized controller is the amount of processing power required to update all the controller coefficients. This also requires a very complex model of the entire system. And a single defect actuator may result in a significant decrease of performance [18].

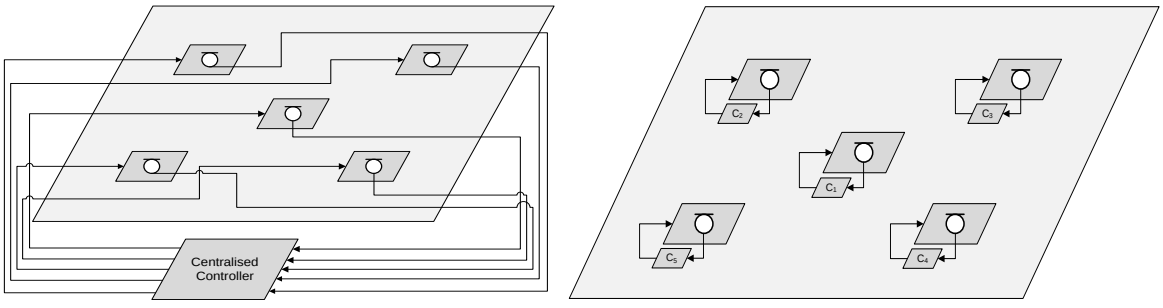

Figure 3 Centralized control and decentralized control

In a decentralized system there is only feedback between every actuator sensor pair (see Figure 3). However, all actuators may excite every sensor. The intuitive condition for stability for a decentralized system requires that the direct coupling in the physical system is larger than the cross-

coupling. A system can thus only be stable if a sensor is closer to the actuator controlling it than to any other actuator. However, this is not a necessary condition for stability. The real upper limit of stability is found by looking at the eigenvalues of the product of the plant transfer matrix and the estimate of the plant transfer matrix which contains only the direct coupling components. If the real parts of all eigenvalues of this resulting matrix are positive then the system is stable [18].

An unstable decentralized system can be made stable by adding a control effort weighting parameter to the cost function of the controllers. But this will be at the expense of a larger steady-state error [18] [13].

HAC/LAC

Feedforward and feedback control can be combined in one system. Such a system contains a high-authority and low-authority control (HAC/LAC) architecture. The main goal of the low-authority feedback control, is to add active damping to the structure. This means that for a multi input multi output system the cross-coupling between the actuator sensor pairs is reduced. The decentralized high-authority feedforward controllers can benefit from this property, because better control at individual points is possible without interfering with other points on the structure. Furthermore, is the robustness to parametric uncertainty of the controller increased by the addition of the low-authority controller and the controller will damp disturbances outside the bandwidth of the harmonic feedforward controller [19] [20]**.**

Recent research

Most papers on feedforward control focus on the control in the principal component space [21]. In these control algorithms, the modes that contribute most to the error are selected and controlled. The other modes are not controlled; the benefit of this method compared to a normal centralized controller is the reduction in computational complexity. This method is, for example, used to reduce the vibrations from gearboxes in helicopters [22] and cars [23].
Many papers use decentralized feedback control to reduce the vibrations of panels [24] [25] [26] [27] [28] [29] [12]. The research in these papers is used in experimental setups; they are not applied to real applications. Only relative old papers focus explicitly on decentralized feedforward control [18] [13].

1.3 Research objective

The goal of this thesis is to implement decentralized adaptive harmonic controller for the double-panel structure. This controller must be stable at all frequencies. Furthermore, should it be as simple as possible. So that only a very limited amount of hardware is required for each controller.

At the start of this thesis a finite element model of the experimental setup was available. With this model the behaviour of the system can be analysed. Therefor first simulations with data of this finite element model are performed. Later the most promising configurations are implemented on the real setup.

In this thesis he following research questions are answered

Examine in simulations if decentralized feedforward control can reduce the sound transmission of the double-panel structure.

On both panels sensors and actuators are installed. Which feedforward configuration reduces the sound transmission the most?

Examine the interaction between feedforward and feedback control. Does this combination Improve the robustness of the system?

Select the best feedforward feedback combination

Find a system identification technique that can initialise the feedforward controllers. This technique should use the components of the feedforward controller as much as possible.

Is a complete decentralized system possible, that can initialise itself without communicating with a centralized controller?

Implement a decentralized controller and test if noise reduction is possible. Also determine if the simulations agree with the practical measurements

Can the decentralized controller react on a disturbance signal with a varying frequency?

How much can the disturbance signal be suppressed by the best control strategy?

1.4 Thesis outline

The ultimate goal of this thesis is to minimise the sound transmission through the double-panel structure with a decentralized adaptive harmonic feedforward controller. To achieve this, first the basics of sound transmission of a structure are studied in chapter2. In this chapter also some acoustic power quantities are introduced. These power quantities are used in later chapters to measure the performance of the system. Chapter 3 focusses on the algorithms of multi-input multi-output harmonic control. In this chapter an adaptive harmonic feedforward controller will be presented. The stability and the convergence rate of this algorithm are analysed. And finally a decentralized algorithm is presented. This chapter will also focus on the detection of the phase and amplitude of the error signals.
In Chapter 4, several system identification techniques are examined. In the last section of this chapter a technique is selected for the double-panel structure.
With the theories and the mathematics presented in the previous three theoretical chapters in the following chapters feedforward controllers and system identification systems are realised and analysed. In Chapter 5, the performance of the adaptive decentralized feedforward controller is analysed in simulations. These simulations use transfer functions from a finite element model of the real-setup. This chapter will prove if it possible to reduce the noise transmission of the double-panel structure with decentralized feedforward control. The best combination of feedforward and feedback control is selected as well.
The created systems which can control the real experimental setup are presented in chapter 6. The system identification system and the feedforward controller are introduced here.
In Chapter 7 experiments on the real setup are performed. A system identification method is developed and compared with a proven method. An adaptive decentralized feedforward controller is

designed and tested. In the conclusion in Chapter 8 the research questions which were defined in in the previous section are answered and some recommendations for further research are made.

2 Acoustics

In this chapter some basic principles in the field of acoustics are treated. These basic principles are required for the analysis of the control of sound radiation from the double-panel structure. The first section is a short introduction to the propagation of waves. This section introduces the basic quantities in acoustic and their dependencies. In the next section acoustic power quantities are introduced. These power quantities are used everywhere in this thesis. In the last section the properties of a vibrating panel are examined. This section will relate the kinetic energy of the panel with its sound radiation. For a more extensive introduction to the field of acoustics see for example Elliott [7] or Fahy [30]

2.1 Propagation of waves

For the transmission of sound a medium is required, in this medium small particles are present that vibrate. A particle oscillates around its original position, it does not travel along with the sound wave. The particles oscillate at a frequency equal to the frequency of the transmitted signal.

A sound wave travels with a velocity, 'the speed of sound', which is not related to the input frequency. Its speed depends on the ambient temperature and the gas constant of the medium. Under normal circumstances this relation can be represented by the following equation

$$c_0 = \sqrt{\gamma R T_a} \qquad (1)$$

Where c_0 is the speed of sound [m/s], γ is the ratio of specific heats of the gas, R the gas constant [J $K^{-1}$$mol^{-1}$], and Ta the absolute temperature [K]. In air at a temperature of 20 °C, the speed of sound is around 343 m/s. In a fluid the velocity of sound is higher. A sound can be produced by a loudspeaker, if the cone of the speaker oscillates it will compress and rarefied the medium. This will increase and decrease the density immediately in front of the cone. The signal is transmitted through space with the speed of sound. The black dots in Figure 4 represent the air molecules. They are compressed and rarefied in a pattern equal to the output signal of the loudspeaker.

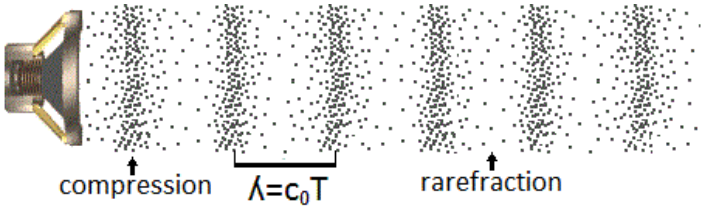

Figure 4 Sound waves.

The distance between two compressions, the wave length λ, is equal to one period of the transmitted signal multiplied by the speed of sound.

Even a very loud noise source generates only small changes in the density of the medium. The ambient density is more than thousand times larger than density fluctuation produced by a very loud

source. Because these changes are so small compared to the ambient value, pressure and density can be considered linearly related. They are related by the following equation:

$$p = c_0^2 \rho \quad (2)$$

where p is the pressure [Pa], ρ is the density [kg/m^3] and c_0 is the speed of sound [m/s]. The particle velocity is also linearly related to the pressure:

$$p = \rho_0 c_0 u \quad (3)$$

In this equation u is the particle velocity and ρ_0 is the ambient density. The product $\rho_0 c_0$ is known as the characteristic acoustic impedance of the medium.

All fluctuations are very small compared to their ambient values and thus linearly related. Therefore, the principle of superposition may be applied to multiple waves which travel through the same medium.

2.2 Acoustic quantities

The variables pressure and particle velocity determine the acoustic power of a wave. In this section all the power quantities used in this report are introduced.

2.2.1 Sound intensity and acoustic power

The sound intensity is defined as the sound power per unit area. The intensity is the product of pressure and particle velocity:

$$\vec{I} = p\vec{u} \quad (4)$$

The particle velocity and sound intensity are vectors, they have a direction and a magnitude. The acoustic power is calculated by integrating the sound intensity over an surface

$$P_{acoustic} = I \cdot A = \frac{|p|^2}{Z} A \quad (5)$$

In free space waves propagate in all directions, every point of a radiating source emits spherical traveling waves in all directions. The acoustic intensity of spherical waves decays by 1/r^2, where r is the distance from the source. This decrease in intensity can be considered a consequence of energy conservation for propagating waves. The energy spreads out over the surface of the expanding sphere. The integral of the sound intensity over the surface of each sphere is equal.

2.2.2 Sound pressure level and sound velocity level

The sound pressure level (SPL) is a logarithmic measure of the sound pressure of a sound relative to a standard reference value. It is measured in decibels (dB) above a standard level:

$$L_p = 10log_{10} \frac{\overline{p^2(t)}}{p_{ref}^2} = 20log_{10} \frac{p_{rms}}{p_{ref}} \quad (6)$$

P_{ref} is a reference pressure of 20 µPa.

Sometimes the velocity is measured instead of the pressure. In this case the sound velocity level (SVL) can be calculated:

$$L_v = 20log_{10}\frac{u_{rms}}{u_{ref}} \quad (7)$$

U_{ref} is the standard reference particle velocity and is equal to $5.0 \cdot 10^{-8}$ m/s [31].

The reference values of the SPL and SVL are scaled in such a manner that both quantities produce approximately the same dB level:

$$\frac{p_{ref}}{u_{ref}} \approx \rho_0 c_0 \longrightarrow L_p \approx L_v \quad (8)$$

2.3 Sound radiation from structures

In this section some basic properties of a vibrating panel are treated. The purpose of this section is to relate the velocity of a panel with its sound radiation. Therefore the kinetic energy of the panel is determined and structural modes are examined.

2.3.1 Kinetic energy

When a panel is excited by an external source it starts vibrating. A vibrating panel radiates with a set of structural modes. Dependent on the frequency of the external source and the dimensions of the structure some modes of the structure will be excited. Each mode has a unique vibrating pattern; a two-dimensional standing wave. The response of the panel is equal to the summation of all modes. Thus, the steady state velocity distribution of a panel can be written as:

$$v(x,y,\omega) = \sum_{n=0}^{\infty} a_n(\omega)\psi_n(x,y) \quad (9)$$

where $a_n(\omega)$ is the amplitude of the m-th mode, and $\psi_n(x,y)$ represents the shape of the mode. The panel vibrates in the direction orthogonal to its surface. For a panel of dimensions L_x by L_y with edges that can not have any linear motion the structural mode shapes are given by

$$\psi_n(x,y) = 4sin\left(\frac{n_1\pi x}{L_x}\right)sin\left(\frac{n_2\pi y}{L_y}\right) \quad (10)$$

where n_1 and n_2 are the modal integers. The structural mode with $n_1 = 1$ and $n_2 = 3$ is referred to as the (1,3) mode. In figure xxx the shapes of some of these modes are shown.

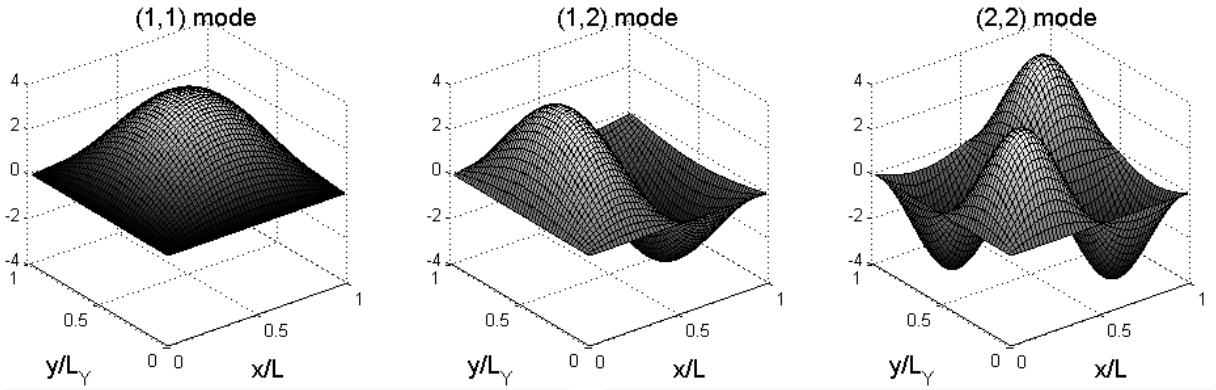

Figure 5 Structural modes of a vibrating panel.

The total kinetic energy of the panel is equal to the total mass multiplied by the mean-square velocity. Its equation, is shown below

$$E_k(\omega) = \frac{M}{4S}\int_s |v(x,y,\omega)|^2 dxdy \quad \textbf{(11)}$$

where S is the surface area of the panel. The mean squared surface integral of the shape of a structural mode has the property that it is equal to one

$$\frac{1}{S}\int_s \psi_n(x,y)^2 dxdy = 1 \quad \textbf{(12)}$$

Thus by combing equation (9) and (11), the kinetic energy can also be written as a summation of the amplitudes of the structural modes times the mass of the panel

$$E_k(\omega) = \frac{M}{4}\sum_{n=0}^{\infty} |a_n(\omega)|^2 \quad \textbf{(13)}$$

Each structural mode has a self radiation efficiency, this efficiency relates the amplitude of the structural mode with the radiated power. The efficiency of a structural mode is determined by its shape and by the excitation frequency. Especially structural modes that have a net volumetric component are efficient. These are the modes that have an odd modal integer, for example, the (1,3) mode. Modes with an even modal integer radiate much less efficient, for these modes the air in front of the panel can transfer from one side of the panel to the other, which will not result in a sound field.

2.3.2 Radiated sound power

The sound fields of different structural modes interact. If the panel vibrates with two modes there is a mutual radiation efficiency. Besides the original self radiation efficiency, an extra component is radiated. The radiated sound power is related by the amplitudes of the structural modes by the following equation

$$\Pi_r = \boldsymbol{a}^H \boldsymbol{M} \boldsymbol{a} \quad \textbf{(14)}$$

where **a** is the vector of all mode amplitudes and matrix **M** contains all radiation efficiencies. The diagonal terms are the self radiation efficiencies and the off-diagonal terms are the mutual radiation efficiencies.

If the panel is lightly damped and excited close to the resonance frequency of the m-th mode, then only this structural mode will contribute significant to the kinetic energy of the panel. Excitation in the region between resonance frequencies will excite all modes a little. At these frequencies almost no reduction in radiation power is possible.

Excitation frequencies with wavelength smaller than the dimensions of the panel will excite multiple modes of the panel. Thus, for low frequencies the far-field sound radiation of a plate is proportional to the kinetic energy of the panel.

2.3.3 Controlling a radiating panel

The kinetic energy of a panel can be measured by installing a couple of acceleration sensors on the panel. If these sensors are well distributed, the amplitudes of the structural modes can be derived

from their output. However, in most applications the kinetic energy is estimated by using equation (11).

In theory, with structural actuators the velocity of the structure can be cancelled. In this situation the panel has no kinetic energy, thus no sound is radiated. In practise, however, the vibration can often only be reduced by the action of secondary actuators, and minimising the total kinetic energy of a structure does not generally result in the minimisation of radiated sound. In fact a reduction of vibration may be accomplished by an increase in sound radiation.

3 Adaptive Harmonic Decentralized Feedforward Controller

This chapter starts with a basic harmonic feedforward control algorithm, each section this algorithm is extended till a decentralized adaptive harmonic feedforward controller is obtained. The stability and convergence rate of the controllers is analysed. Control effort weighting is added to the algorithms to stabilize them. In the principle component space the effect of effort weighting is examined. The last sections of this chapter focus on the detection of the harmonic error signals.

3.1 Harmonic feedforward controller

In Figure 6 the most basic active noise control system is shown. An external source produces a single tone deterministic disturbance signal d(n). This disturbance signal is measured by microphone, which is connected to the active noise control system. The measured signal is called the error signal, e(n).

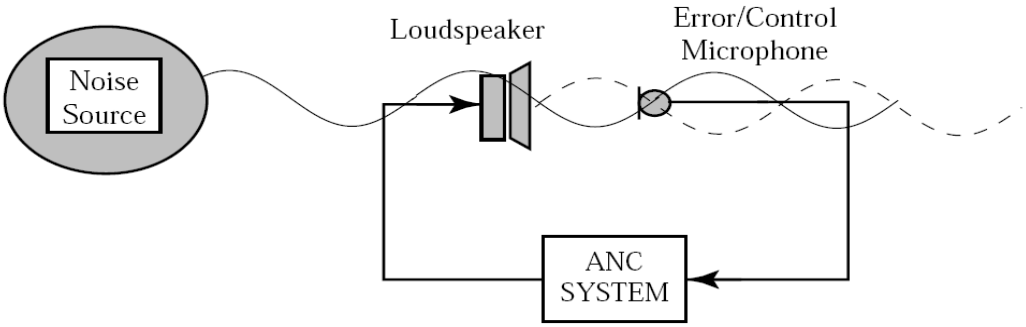

Figure 6 The principle of anti-sound.

The controller will try to produce a control signal, u(n), that will completely cancel the disturbance signal at the microphone. The active noise control system will succeed in this task if it knows the complex transfer function between the loudspeaker and microphone. This transfer function, G, is called the complex frequency response of the plant. The error signal can thus be written as follows

$$e(n) = d(n) + Gu(n) \quad \textbf{(15)}$$

The disturbance signals of the propeller engines contain multiple tones. And beside these tones background noise is present in the measured signal. However, a controller very similar to the above mentioned method can be created in the frequency domain. The sampled periodic disturbance signal of the propeller engines can be represented as a finite summation of its harmonics

$$d(n) = \sum_{k=-K}^{K} D_k e^{jk\omega_0 Tn} \quad \textbf{(16)}$$

where k is the harmonic number, D_k is the complex amplitude of the k-th harmonic.

The control algorithm can be divided in K independent loops, each operating on an individual harmonic. Our application only needs to control a couple of harmonics. All other harmonics are not processed. In Figure 7, a harmonic controller in the frequency domain is shown.

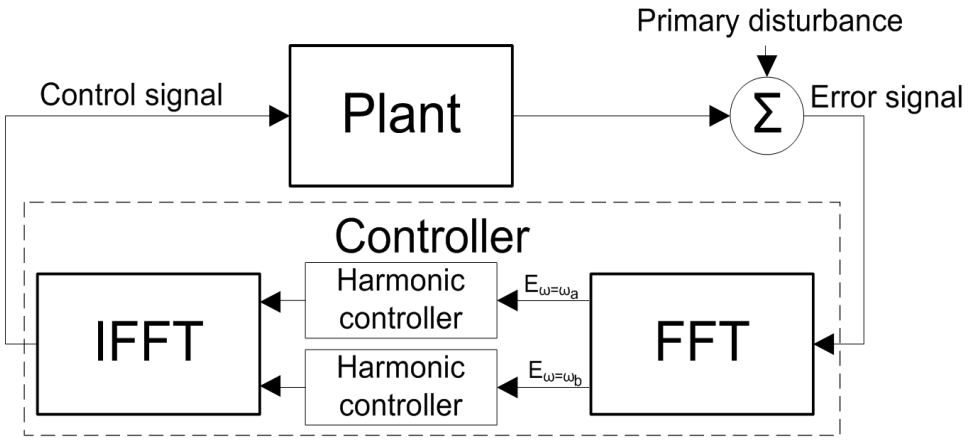

Figure 7 An implementation of the frequency-domain harmonic controller.

This controller uses a Fast Fourier Transformation to transform the error signal to the frequency domain. Then a couple of harmonics are selected which are processed independently. The resulting control signals are joined and transformed back to the time domain. The error of the k-th harmonic can be written as

$$E_k = D_k + G\left(e^{jk\omega_0 T}\right)U_k \qquad \textbf{(17)}$$

The optimal control signal for this harmonic is:

$$U_{k,opt} = -\frac{D_k}{G(e^{jk\omega_0 T})} \qquad \textbf{(18)}$$

The double-panel structure has multiple sensors and multiple actuators. Therefore, a multichannel feedforward control system in required instead of a single channel feedforward control system. In Figure 8, a single panel of the structure with its five piezoelectric actuators is shown. On the actuators the sensors are mounted. Activating actuator one, will make the entire panel vibrate. All sensors will measure a response.

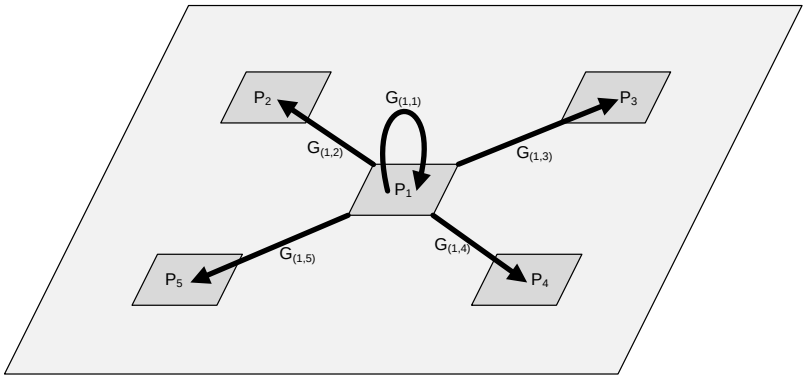

Figure 8 Mulitchannel plant response.

Also the disturbance signal has a transfer function to all error sensors. For a multichannel system equation (17) is extended to a vector form

$$\boldsymbol{E}_k = \boldsymbol{D}_k + \boldsymbol{G}\left(e^{jk\omega_0 T}\right)\boldsymbol{U}_k \quad \textbf{(19)}$$

where **G** is a matrix of the complex plant responses. All other elements are vectors.

Not in all applications it is possible to produce control signals equal to its optimal value. For example, the control signals might be limited to an upper bound. As a result not all disturbance signals are cancelled at the error sensors. The problem of finding the optimal value for the control signals can be split into L independent optimisation problems. However, most of the time a general formulation is used which weights all error signals equal. Its cost function is defined as the sum of the square error signals

$$J(n) = \boldsymbol{E}(n)^H \boldsymbol{E}(n) \quad \textbf{(20)}$$

3.2 Adaptive harmonic feedforward controller

The harmonic feedforward controller presented in the previous section works only under perfect circumstances. In practise, due to environmental changes the responses might change over time. Temperature changes for example, change the speed of sound (see section 2.1) which will change the phase of the received signals. Instead of cancelling the disturbance signal it might now be amplified. Also small measurement errors of the re

Therefore, in this section an iterative algorithm for adjusting the control signals is presented, the steepest descent algorithm. This algorithm updates the control signals at each iteration in proportion with the negative gradient of the cost function with respect to these control variables. This way, the algorithm will converge to the optimal solution. The steepest descent algorithm is shown below

$$\boldsymbol{U_k}(n+1) = \boldsymbol{U_k}(n) - \mu \frac{dJ}{d\boldsymbol{U_k}(n)} \quad \textbf{(21)}$$

where J is the cost function, n is the iteration index, and μ is the convergence factor. The derivative of the cost function is called the complex gradient vector, and can be written as

$$\boldsymbol{g_k}(\boldsymbol{n}) = \frac{dJ(n)}{d\boldsymbol{U_k}(n)} = \boldsymbol{2G^H E_k}(n) \quad \textbf{(22)}$$

Combining equations (21) and (22) results in the following algorithm

$$\boldsymbol{U}_k(n+1) = \boldsymbol{U}_k(n) - \propto \boldsymbol{G}^H \boldsymbol{E}_k(n) \quad \textbf{(23)}$$

in which $\propto = 2\mu$ is the convergence coefficient

By combing equation (23) and (19) the following equation for the control signal is obtained

$$\boldsymbol{U}(n+1) = \boldsymbol{U}(n) - \propto [\boldsymbol{G}^H \boldsymbol{D}(n) + \boldsymbol{G}^H \boldsymbol{G}\boldsymbol{U}(n)] \quad \textbf{(24)}$$

This equation will reach a steady-state solution when **U**(n+1) is equal to **U**(n). The term in the square brackets is zero under these circumstances. The optimal control signal is thus equal to:

$$\boldsymbol{U}_{\boldsymbol{opt}} = -\frac{\boldsymbol{D}}{\boldsymbol{G}} \quad \textbf{(25)}$$

This is equal to the optimal solution of the non-adaptive feedforward controller.

The drawback of an adaptive controller is that the algorithm only converges to its optimal solution if a number of conditions are met. In an unstable system a certain parameter of the system cannot be controlled from the outside. This will result in an uncontrollable output signal, which can reach an unlimited value. The input signal will not be able to influence this output.

The convergence of the algorithm can be examined by combining equation (24) and (25)

$$\boldsymbol{U}(n+1) - \boldsymbol{U}_{\boldsymbol{opt}} = (\boldsymbol{I} - \propto \boldsymbol{G}^H \boldsymbol{G})\big(\boldsymbol{U}(n) - \boldsymbol{U}_{\boldsymbol{opt}}\big) \quad \textbf{(26)}$$

Equation (26) can be rewritten to the following form, assuming **U**(0)=**0**

$$\boldsymbol{U}(n) - \boldsymbol{U}_{\boldsymbol{opt}} = -(\boldsymbol{I} - \propto \boldsymbol{G}^H \boldsymbol{G})^n \boldsymbol{U}_{\boldsymbol{opt}} \quad \textbf{(27)}$$

The control signal can only obtain its optimal value if equation (27) converges. The convergence of this equation is determined by the eigenvalues of the matrix $\mathbf{G^H G}$. This matrix is called the Hessian matrix, and it is the second derivative of the cost function with respect to the control signal. The real parts of all the eigenvalues must be positive for the equation to converge.

Furthermore, there is a limit on the convergence coefficient∝. The steepest descent algorithm will only converge if

$$|1 - \propto \lambda_m| < 1, \quad for\ all\ m \quad \textbf{(28)}$$

The above equation will be proven in the principal component space in section 3.6. For complex eigenvalues this equation can be written as

$$0 < \propto < \frac{2Re(\lambda_m)}{|\lambda_m|^2}, \quad for\ all\ m \quad \textbf{(29)}$$

3.3 Control effort weighting

In this section a method is presented which can make an unstable system stable.

An unstable system can become stable by the addition of a control effort weighting factor in the control law. The cost function for this system is defined as follows

$$J(n) = \boldsymbol{E}(n)^H \boldsymbol{E}(n) + \beta \boldsymbol{u}(n)^H \boldsymbol{u}(n) \quad \textbf{(30)}$$

This cost function will not minimise the squared error signals, but a combination of the squared error signal and the squared control signals. So the optimal solution of this cost function will not cancel all disturbance signals. The derivate of the cost function, the complex gradient vector, is shown below

$$\boldsymbol{g}(n) = \frac{dJ(n)}{d\boldsymbol{U}(n)} = 2\boldsymbol{G}^{\boldsymbol{H}} \boldsymbol{E}_{\boldsymbol{k}}(n) + \beta \boldsymbol{u}(n) \quad \textbf{(31)}$$

The steepest descent algorithm with control effort weighting is shown in the equation below

$$\boldsymbol{U}(n+1) = (1 - \alpha\beta)\boldsymbol{U}(n) - \alpha \boldsymbol{G}(n)^H \boldsymbol{E}(n) \quad \textbf{(32)}$$

By following the same steps as in the previous section the optimal control signal of this algorithm is derived

$$\boldsymbol{U_{opt}} = -[\boldsymbol{G}^{\boldsymbol{H}} \boldsymbol{G} + \beta \boldsymbol{I}]^{-1} \boldsymbol{G}^{\boldsymbol{H}} \boldsymbol{D} \quad \textbf{(33)}$$

And the convergence of the algorithm depends on, assuming that **U**(0)=**0**

$$\boldsymbol{U}(n) - \boldsymbol{U_{opt}} = -(\boldsymbol{I} - \propto [\boldsymbol{G}^H \boldsymbol{G} + \boldsymbol{\beta I}])^n \boldsymbol{U_{opt}} \quad \textbf{(34)}$$

The addition of the control effort weighting factor changes the eigenvalues of the system to the following values

$$\lambda'_m = \lambda_m + \beta \quad \textbf{(35)}$$

Thus by adding a control effort weighting factor an unstable system with negative eigenvalues can be made stable. Hence, the minimum required control effort weighting is

$$\beta_{min} = \max(\lambda_{min}, 0) \quad \textbf{(36)}$$

The convergence criteria presented in the previous section is still valid for this system, however the new eigenvalues should be used in the equation. In section 3.6.2 the effect of effort weighting on the average squared error will be demonstrated.

3.4 Decentralized controller

In this section decentralized control and the effect of plant uncertainties are introduced. From the theory of the latter the effect of decentralized control can be derived.

3.4.1 Effect of plant uncertainties

As was shown in equation (32)**,** a steepest descent algorithm with effort weighting can be used to control the system to a minimum error solution when the phase and amplitude of the disturbance signal are unknown. However, in reality the response of the plant **G** is not known exactly. Thus, instead of **G** an estimate of the plant response function is used, $\widehat{\boldsymbol{G}}$. This uncertainty might change the

behaviour of the adaptive algorithm, the system might become unstable and a different finale state may be reached. The steepest descent algorithm with effort weighting and plant uncertainty is shown below

$$\boldsymbol{U}(n+1) = (1-\alpha\beta)\boldsymbol{U}(n) - \alpha\widehat{\boldsymbol{G}}^{H}\boldsymbol{E}(n) \quad \textbf{(37)}$$

The addition of plant uncertainty to the steepest descent algorithm changes the optimal steady state control effort to

$$\boldsymbol{U_{opt}} = -\left[\widehat{\boldsymbol{G}}^{H}\boldsymbol{G} + \beta\boldsymbol{I}\right]^{-1}\widehat{\boldsymbol{G}}^{H}\boldsymbol{d} \quad \textbf{(38)}$$

3.4.2 Decentralized controller

From the model of uncertainty in the plant response estimation a decentralized control algorithm can be derived. If the elements of the plant response matrix **G** are known or can be reliably measured, $\widehat{\boldsymbol{G}}$ can be set equal to the diagonal elements of **G**. Hence, each control signal is only updated by one error signal. This means that there are now k independent controllers, with an actuator sensor pair and they only know the response function between these two elements. For a system with three actuator sensor pairs the estimated plant response is thus given by

$$\widehat{\boldsymbol{G}} = \begin{bmatrix} g_{11} & 0 & 0 \\ 0 & g_{22} & 0 \\ 0 & 0 & g_{33} \end{bmatrix} \quad \textbf{(39)}$$

When $\boldsymbol{G}$ and $\widehat{\boldsymbol{G}}$ are known the stability of the system can be calculated. The same rules for stability apply for a decentralized system as for a centralized system, the eigenvalues of the matrix ($\widehat{\boldsymbol{G}}^{H}\mathbf{G}+\beta\mathbf{I}$) must be positive. Else will the adaptive algorithm given in equation (34) will not converge. Because the decentralized plant response estimation matrix $\widehat{\boldsymbol{G}}$ contains only diagonal elements, the system will be more unstable and require larger effort weighting to become stable.

3.5 Gersgorin's Theorem

With Gersorin's theorem the location of the eigenvalues are estimated. This technique might be useful for decentralized application. Because it does not require knowledge of the complete complex frequency response matrix at each decentralized location. In this section this method is demonstrated.

3.5.1 The theorem

In the equation below a square matrix **A** is given:

$$\boldsymbol{A} = \begin{bmatrix} a_{11} & \cdots & a_{1n} \\ \vdots & \ddots & \vdots \\ a_{n1} & \cdots & a_{nn} \end{bmatrix} \quad \textbf{(40)}$$

Every eigenvalue of this matrix satisfies at least one of the inequalities:

$$|\lambda - a_{ii}| \leq \sum_{\substack{j=1 \\ j\neq i}}^{n} |a_{ij}| \quad \textbf{(41)}$$

Thus, each row of matrix **A** gives information on the location of a single eigenvalue. This eigenvalue will lie inside a circle region which is centred at a_{ii} and has a radius equal to the sum of all other elements of that row.

If a square matrix is transposed, then its eigenvalues do not change. Thus, equation (41) is also valid for the columns:

$$|\lambda - a_{ii}| \leq \sum_{\substack{j=1 \\ j \neq i}}^{n} |a_{ji}| \qquad \textbf{(42)}$$

By combining these two methods an even better assumption of the eigenvalues can be made. Let's illustrate this theorem with a small example. For the square matrix **A** the following values are chosen:

$$\boldsymbol{A} = \begin{bmatrix} 1 & 0 & -1 \\ 0 & 3 & 2 \\ 0 & 1 & 7 \end{bmatrix}$$

The diagonal elements of this matrix are the centres of the circles, in which the eigenvalues must lay. The sum of the non-diagonal elements in the associated row or column determines the radius of the circle. This is shown in Figure 9.

Eigenvalue region rows

Center	Radius
1	1
3	2
7	1

Eigenvalue region columns

Center	Radius
1	0
3	1
7	8

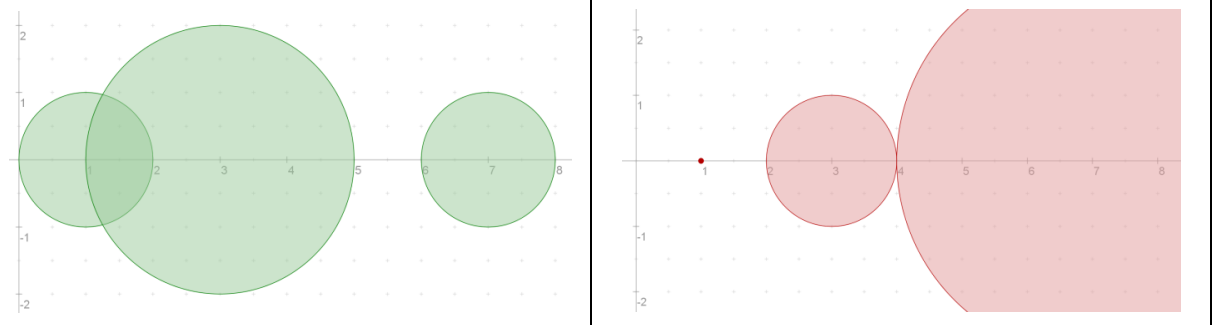

Figure 9 Eigenvalue regions

The blue circles in Figure 10, represent the regions of the eigenvalues if both methods are combined. As you can see, combining these two methods can result in a significant improvement in estimating the eigenvalues.

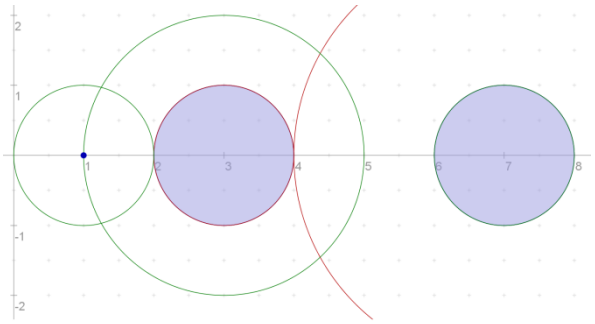

Figure 10 Combined eigenvalue regions

The estimation of the region in which the eigenvalues must lie can be further improved by applying a similarity transformation. There are however, an unlimited amount of similarity transformations possible which all can be combined whit each other.

An equivalent matrix of **A** can be created by applying the similarity transformation $\mathbf{TAT}^{-1}$. This transformation creates a matrix which has the same eigenvalues as the original matrix **A**.

$$\boldsymbol{TAT}^{-1} = \begin{bmatrix} \rho_1 & 0 & 0 \\ 0 & \rho_2 & 0 \\ 0 & 0 & \rho_3 \end{bmatrix} \begin{bmatrix} a_{11} & a_{12} & a_{13} \\ a_{21} & a_{22} & a_{23} \\ a_{31} & a_{32} & a_{33} \end{bmatrix} \begin{bmatrix} 1/\rho_1 & 0 & 0 \\ 0 & 1/\rho_2 & 0 \\ 0 & 0 & 1/\rho_3 \end{bmatrix}$$
$$= \begin{bmatrix} a_{11} & \frac{\rho_1}{\rho_2} a_{12} & \frac{\rho_1}{\rho_3} a_{13} \\ \frac{\rho_2}{\rho_1} a_{21} & a_{22} & \frac{\rho_2}{\rho_3} a_{23} \\ \frac{\rho_3}{\rho_1} a_{31} & \frac{\rho_3}{\rho_2} a_{32} & a_{33} \end{bmatrix} \quad \textbf{(43)}$$

From this result the following equation is derived, every eigenvalue of this matrix satisfies at least one of the inequalities:

$$|\lambda - a_{ii}| \leq \sum_{\substack{j=1 \\ j \neq i}}^{n} \frac{\rho_i}{\rho_j} |a_{ij}| \quad \textbf{(44)}$$

3.5.2 Gersgorin's theorem and decentralized control

With Gersgorin's theorem each decentralized controller can calculate its own control effort weighting factor. For this calculation it only requires the complex transfer functions from all actuators to its own sensor.

The convergence of the adaptive decentralized feedforward algorithm with effort weighting is determined by the eigenvalues of the matrix $\hat{\mathbf{G}}^{\mathbf{H}}\mathbf{G} + \beta\mathbf{I}$. Applying Gersgorin's theorem on this matrix will result in a stability matrix **A**, which has the diagonal elements:

$$a_{ii} = |g_{ii}|^2 + \beta \quad \textbf{(45)}$$

which are real and positive, the off-diagonal elements being

$$a_{ij} = g_{ii}^{*} g_{ij} \quad \textbf{(46)}$$

By using equations (45),(46) and(41) the following law can be derived, which guarantees stability

$$|g_{ii}|^2 + \beta \geq \sum_{\substack{j=1 \\ j \neq i}}^{M} |g_{ii}^* g_{ij}|, \quad for\ all\ i \qquad \textbf{(47)}$$

This equation can be rewritten in the following form

$$|g_{ii}| + {}^{\beta}\!/_{|g_{ii}|} \geq \sum_{\substack{j=1 \\ j \neq i}}^{M} |g_{ij}|, \quad for\ all\ i \qquad \textbf{(48)}$$

As explained earlier in this section a region is calculated in which the eigenvalues may lie. Thus, Equation (48) provides a sufficient condition for the stability of a decoupled system, but not a necessary one. It is possible that equation (48) is not satisfied and yet the system is stable.

3.6 Principal component analysis

In this section the complex plant response will be transformed to its principal components. This will result in a new block diagram and a new formulation of the cost function. The principal component form provides more insight in the behaviour of the system. With this information the effect of effort weighting is demonstrated. Also the algorithm will be investigated, to show if it can be used in a decentralized control system.

3.6.1 The algorithm

In a multichannel control system, different modes are excited by the disturbance signal. By transforming the complex plant response to its principal components the contribution to the error signal of each individual component can be determined. Each component has its own power and its own convergence rate.

The singular value decomposition of the complex plant response of a system with L error sensors and M actuators is defined as

$$\boldsymbol{G = R\Sigma Q^H} \qquad \textbf{(49)}$$

The unitary matrix R contains the complex eigenvectors of GG^H and the unitary matrix Q contains the complex eigenvectors of G^HG. The L columns of R and the M columns of Q are called the left singular values and the right singular values, respectively. Σ represent the singular values matrix, this is an L by M matrix, the diagonal components contain the singular values all other elements are equal to zero. The singular values, σ_m, are sorted by size; the upper left element of the matrix contains the largest singular value. The singular values are equal to the square roots of the eigenvalues, λ_m, of the matrix G^HG or GG^H

$$\sigma_m = \sqrt{\lambda_m} \qquad \textbf{(50)}$$

The complex Hessian matrix can be expressed as

$$\boldsymbol{G^H G = Q\Sigma^T \Sigma Q^H} \quad \textbf{(51)}$$

Using equations (30),(33),(51) and (52) the optimal control signal without control effort weighting is now given by

$$\boldsymbol{U_{opt} = -Q[\Sigma^T \Sigma]^{-1} \Sigma^T R^H D} \quad \textbf{(52)}$$

By combining equation (15) and (49) and multiplying both sides by R^H the following equation is obtained

$$\boldsymbol{R^H e}(n) = \boldsymbol{R^H d} + \boldsymbol{\Sigma Q^H u}(n) \quad \textbf{(53)}$$

This equation can be transformed to a useful form which is given by

$$\boldsymbol{y}(n) = \boldsymbol{p} + \boldsymbol{\Sigma v}(n) \quad \textbf{(54)}$$

In this equation a few new terms are defined; the transformed input signal **y**(n), the transformed disturbance signal **p** and the transformed control vector **v**(n):

$$\mathbf{y}(\mathrm{n}) = \boldsymbol{R^H e}(n) \quad \textbf{(55)}$$
$$\boldsymbol{p} = \boldsymbol{R^H d} = [p_1, p_2, \dots, p_{L-1}, p_L] \quad \textbf{(56)}$$
$$\boldsymbol{v}(n) = \boldsymbol{Q^H u}(n) \quad \textbf{(57)}$$

In Figure 11 the block diagram of this transformed system is shown. Because only the diagonal elements of the matrix ∑ contain a value that is non-zero, every transformed error signal y is only a function of a single transformed disturbance function and a single transformed control signal (when the number of sensors and actuators is equal).

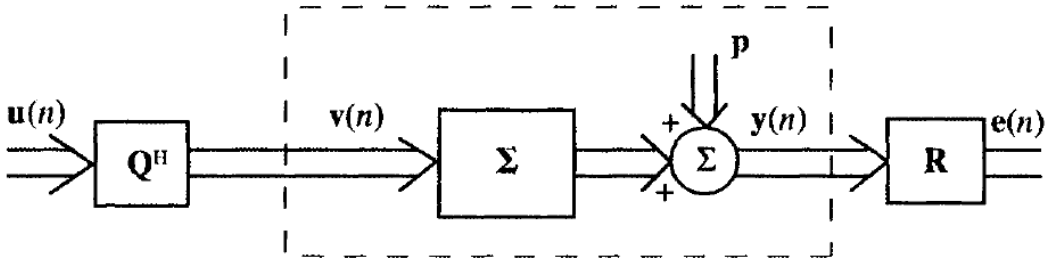

Figure 11 Principal component block diagram of a multichannel tonal control system.

By minimalizing all the independent components of **y**(n) the error signal **e**(n) is minimalized as well . Thus the optimal values for the individual transformed control signals are:

$$v_{m:opt} = -p_m/\sigma_m \quad \textbf{(58)}$$

Because the matrix **R** is unitary the cost function can be written as a function of **y**(n)

$$\boldsymbol{J = e^H e = y^H y} = \sum_{m=1}^{L} |y_m|^2 \quad \textbf{(59)}$$

The behaviour of a system which is transformed to its principal components is not changed. So the convergence behaviour is still the same. The benefit of this transformation is that the individual components of the error signal are better observable and controllable. With this transformation it is possible to only control the principle components that contribute most to the error signal. The other principal components will just be ignored, and so not proportional high control signals can be avoided.

The adaptive feedforward algorithm of equation (23) is written in the principal component form as follows:

$$\boldsymbol{v}(n+1) = \boldsymbol{v}(n) - \propto \Sigma^T \boldsymbol{y}(n) \quad \textbf{(60)}$$

Because $\sum$ is a matrix with only diagonal elements the above equation van be written as M independent equations:

$$v_m(n+1) = v_m(n) - \alpha\sigma_m y_m(n) \quad \textbf{(61)}$$

By combing equations (61),(58) and (54) and using the fact that ${\sigma_m}^2 = \lambda_m$ the following equation is obtained

$$\left(v_m(n) - v_{m:opt}\right) = (1 - \alpha\lambda_m)^n \left(v_m(0) - v_{m:opt}\right) \quad \textbf{(62)}$$

The limitation on the convergence coefficient α as shown in section 3.2 is proven by the above equation.

The convergence behaviour of the cost function is shown below. Every mode converges independently. Of course only the modes which are controlled will converge, the modes that are not controlled will always contribute $|p_m|^2$ to the cost the function.

$$J(n) = \sum_{m=1}^{L} |p_m|^2 \, e^{-2\alpha\lambda_m n} \quad \textbf{(63)}$$

3.6.2 Effort weighting

As explained in section 3.2 only modes with a positive eigenvalue will converge (see for example equation (63)). Systems with negative eigenvalues are unstable and must be made stable by adding effort weighting. In the principal component form effort weighting is added as follows:

$$\boldsymbol{G^H G} + \beta \boldsymbol{I} = \boldsymbol{Q}[\boldsymbol{\Sigma^T \Sigma}] + \beta \mathbf{I}]\boldsymbol{Q^H} \quad \textbf{(64)}$$

The optimal control signal is obtained by a similar derivation as in the previous section

$$\boldsymbol{U_{opt}} = -\boldsymbol{Q}[\boldsymbol{\Sigma^T \Sigma}] + \beta \mathbf{I}]^{-1} \boldsymbol{\Sigma^T P} \quad \textbf{(65)}$$

By combining multiple equations (see Elliott [13]) it can be shown that the minimum mean squared error is equal to

$$(\boldsymbol{E^H E})_{opt} = \sum_{m=1}^{L} \frac{\beta^2}{\sigma_m^2 + \beta^2} |p_m|^2 \quad \textbf{(66)}$$

3.6.3 Conclusion

The principal component form gives a good overview of the effect of effort weighting. Modes for which $\sigma_m^2 \ll \beta^2$ will not have their contribution to the sum of the squared errors removed by the control algorithm. A suitably chosen value of β will not only make the system stable, but can also prevent physically unreasonable values of control effort.

Some applications only control the modes that contribute most to the total error. A decentralized implementation of such a system is not possible. Modes are not related to sensor actuator pairs. A system that controls only a couple of modes requires the information of all sensors, and has to control all actuators. This information can only be processed by a centralized controller.

3.7 Phasor arithmetic

In a harmonic controller all calculations are performed with phasors. A phasor is a representation of a sine wave whose amplitude and angular frequency are time-invariant. Phasors decompose the behaviour of a sinusoid into two components; amplitude and phase.

The sensors of the system measure a continuous time error signal, which is assumed to have a constant frequency and amplitude, this signal is transformed to a phasor. Then some calculations are performed, which will result in a control signal in phasor form. This phasor is transformed back to a continuous time signal and transmitted by the actuator. In this section the best methods for these phasor operations are examined.

All sinusoid signals have a phase and amplitude. In the equation below, a cosine is written as a complex signal:

$$A \cdot \cos(\omega t + \theta) = Re\{Ae^{i\theta} \cdot e^{i\omega t}\} \quad \textbf{(67)}$$

In this equation $Ae^{i\theta}$ is the phasor. A phasor can be stored with an amplitude and phase component or with a real and imaginary component.

Two complex numbers are multiplied as follows (using real and imaginary components):

$$z_1 z_2 = (a + bi)(c + di) = (ac - bd) + (bc + ad)i \quad \textbf{(68)}$$

This equation can be modified to a form that uses only three distinct multiplications to calculate the real and imaginary part [32]. This new formulation requires a few extra additions, however on most systems the computational cost of additions is much less than multiplications.

$$z_1 z_2 = [ac - bd] + [(a + b)(c + d) - ac - bd]i \quad \textbf{(69)}$$

The process of multiplying two complex numbers is best visualised in polar coordinates. The complex signal can be converted to a magnitude and phase signal.

$$z_1 = A_1[cos(\theta_1) + i\, sin(\theta_1)] \quad \textbf{(70)}$$

And two complex numbers in polar coordinates can be multiplied as follows:

$$z_3 = z_1 z_2 = r_1 r_2 [cos(\theta_1 + \theta_2) + i\, sin(\theta_1 + \theta_2)] \quad (71)$$

In polar coordinates only two operations are required, the magnitudes of the two signals are multiplied and the two phases are added to each other. However, addition is much harder in polar coordinates. For an addition operation the signals need to be transformed to complex numbers before they can be added. This is shown in the equation below:

$$A_3^2 = \big(A_1 cos(\theta_1) + A_2 cos(\theta_2)\big)^2 + \big(A_1 sin(\theta_1) + A_2 sin(\theta_2)\big)^2 \quad (72)$$

$$\theta_3 = arctan\left(\frac{A_1 sin(\theta_1) + A_2 sin(\theta_2)}{A_1 cos(\theta_1) + A_2 cos(\theta_2)}\right) \quad (73)$$

3.8 Error signal detection

The error signal produced by a rotating propeller consists only of a few frequency components. Its main error component is equal to the blade passage frequency. The other excited frequencies are higher harmonics of this fundamental frequency. The harmonic controller only has to know the errors of these frequencies. In other frequencies the controller is not interested. In this section, three techniques are presented for the detection of the phase and the magnitude of these error components. In the final part of this section, these techniques are compared and the best solution is chosen.

3.8.1 Fast Fourier Transformation (FFT)

A Fast Fourier transformation (FFT) measurement of the spectrum has two possible sources of errors. The first one is the aliasing error, the power of higher frequencies is mirrored at the lower frequencies. This can be avoided by setting the sample frequency higher than 2 times the highest frequency present in the measurement signal. Generally it is advised to low pass filter the measurement signal before applying a FFT operation. The second source of error is called the leakage error, single frequencies will be smeared out in neighbouring frequency bins. This error appears if no integer number of periods of the excitation signal is measured. This problem can be avoided by changing the configurations of the measurement setup, for example by adjusting the duration or the sample time of your system. If this is not possible the error can be minimized by using a window other than a rectangular window. In general, a window will smoothly weight the first and last samples of a measurement less heavy in order to decrease the discontinuities of the measurement signal.

The spectrum is split in different frequency bins. This introduces another limitation, the desired signal must be exactly centred in a frequency bin. Else its power is spread into the two closest bins.

The FFT algorithm has to gather all N samples before it can calculate the spectrum. Thus, it has to store all these samples temporarily.

3.8.2 Goertzel algorithm

The Goertzel algorithm identifies only a single predefined frequency component of a signal. While an FFT analyses the entire spectrum. Multiple implementations of this algorithm are required to measure multiple frequency components. The Goertzel algorithm computes the following sequence:

$$s(n) = x(n) + 2\cos(2\pi\omega) \cdot s(n-1) - s(n-2) \quad (74)$$

where (s-2) and s(-1) are equal to zero. From this sequence the phasor of the signal can be derived with the following equation

$$X(\omega) = e^{2\pi i\omega} s(n-1) - s(n-2) \quad \textbf{(75)}$$

A great advantage of this algorithm compared to the FFT is that there is no leakage error. Thus an arbitrary length of the measurement can be chosen. This reduces the complexity of the measurement setup. Also the algorithm can process samples as they arrive. Only when all samples are received a small extra operation is required to calculate the phasor.

The frequency resolution of the Goertzel algorithm is the same as for the FFT. Thus, the same number of samples is required to remove the effect of undesired neighbouring frequency components.

3.8.3 Linear Least Square (LLS) technique for phase estimation

The LLS phase estimation technique uses a maximum likelihood (ML) approach for an optimum estimation of the phase and amplitude of the signal. This method can find multiple frequency components with a single operation.

A signal that consists of M sinusoids can be written as follows:

$$x(n) = \sum_{m=1}^{M} A_m \cos(\omega_m n + \phi_m) \quad \textbf{(76)}$$

where $A_m>0$, $\omega_m \in (0,\pi)$ and $\phi_m \in (-\pi,\pi)$ denote the amplitude, frequency and phase of the m-th sinusoid. The cosine term of a single sinusoid can be written as the product of two vectors:

$$A_m \cos(\omega_m n + \phi_m) = [\cos(\omega_m n) \quad -\sin(\omega_m n)\,] \begin{bmatrix} A_m \cos(\phi_m) \\ A_m \sin(\phi_m) \end{bmatrix} \quad \textbf{(77)}$$

Notice that the second vector is not dependent on n, and contains all phase and amplitude information of the signal.

Each measurement N samples are measured. And from these samples the phase and amplitude are derived. Equation (77), can be rewritten as a vector of N samples:

$$\boldsymbol{x} = \boldsymbol{H\alpha} \quad \textbf{(78)}$$

where $\boldsymbol{x} = [x_0\ x_1\ \ldots.\ x_{N-1}\ x_N]^T$, **α** is a 2 by 1 vector and **H** is a N by 2 matrix. In this equation **H** is a reference signal with which the input signal is compared. The phase and amplitude differences are stored in **α**. The reference signal **H** has the following format:

$$\boldsymbol{H} = \begin{bmatrix} A_1 cos(\varphi_{ref}) & A_1 sin(\varphi_{ref}) \\ A_1 cos(\omega_1 + \varphi_{ref}) & A_1 sin(\omega_1 + \varphi_{ref}) \\ \vdots & \vdots \\ A_1 cos((N-1)\omega_1 + \varphi_{ref}) & A_1 sin((N-1)\omega_1 + \varphi_{ref}) \end{bmatrix} \quad \textbf{(79)}$$

where A_1 and φ_{ref} are the reference amplitude and phase. Thus, to find the phase and amplitude of the input signal **x**, parameter **α** must be estimated. The LLS estimate for **α** is computed as:

$$\hat{\boldsymbol{\alpha}} = (\boldsymbol{H}^T\boldsymbol{H})^{-1}\boldsymbol{H}^T\boldsymbol{x} \quad \textbf{(80)}$$

The LLS method calculates $(\mathbf{H}^T\mathbf{H})^{-1}$ for each measurement. If the reference signal is the same for each measurement this has to be done only once. By extending the vectors multiple signal components can be detected (see So [33]). The detection of multiple frequency components will increase the size of the matrix $\mathbf{H}^T\mathbf{H}$, this will significantly increase the complexity of the inverse operation performed on this matrix.

The accuracy of this method is equal to the Goertzel algorithm. If these two algorithms are tuned to detect only a single frequency component their frequency responses are exactly the same.

3.8.4 Comparison

The disturbance measured by the sensors can obtain any frequency within a certain range, and this frequency may change over time. The FFT method is not flexible enough for this situation. It can not centre a frequency component in a frequency bin for all situations. This will introduce unacceptable large errors in the estimation. Therefore, only the Goertzel algorithm and the LLS phasor estimation method can be used for this application.

In the table below the computational complexity of the different algorithms are shown. Unlike all other methods the LLS method compares its phase to a reference phase. Therefore, this method is considerably less efficient. In this table also the simple DFT method for a single frequency bin is shown.

	Multiplications	Additions / subtractions	Sinusoid function computations
Radix-2 FFT	$2N \log_2(N)$	$3N \log_2(N)$	2N
DFT single frequency bin	2N	2N	2N
Goertzel algorithm	N+2	2N+1	2
LLS phasor estimator	(3+2)N	(3+2)N	2N

In the harmonic controller first the LLS phasor estimator technique will be implemented. This method is chosen because it has the best accuracy and is easy to implement. Later this method will be replaced by the Goertzel algorithm because it is less computational complex and has the same performance.

4 System identification

For optimal control of the double-panel structure the transfer functions between all actuators and sensors in the system must be known. With these transfer functions the control algorithm can be configured. For optimal control it is required that transfer function estimations are accurate, else the system might get unstable.

In this chapter various system identification techniques are presented. These techniques are compared and the best solution is chosen. The important factors in this decision are measurement time and system complexity.

4.1 Possible implementations

The dynamic behaviour of a system can be derived from measurements of the input and output signals. In the double-panel structure it is possible to excite each input with an arbitrary chosen signal. In normal operating mode the decentralized actuator sensor pairs do not need to communicate with each other. Thus, no centralized controller is required. However, in the system identification phase communication between these elements is required, there has to be a mechanism that tells each decentralized controller when it has to listen and when it has to produce a control signal. Else, all components will talk at the same time and no information of the system is obtained. Of course, the best option is to limit the communication between the elements as much as possible. The disadvantage of such systems is that each controller has to calculate complex functions, for which complex hardware is required. This hardware might not be needed in normal operating mode. However, there are also techniques that require less complex hardware but they might be too slow.

The system identification process can be performed with the following three configurations

Decentralized System identification

The first implementation is almost completely decentralized. One after the other, all actuators will produce an excitation signal. During this stage all sensors will listen to the response. This way, all decentralized controllers will know the response from all actuators to their sensor. According to Gersgorin's theorem this is enough for a stable system. With this information they can calculate their own values for alfa and beta

Decentralized data analysis, centralized parameter calculation

This implementation uses the same techniques to determine the transfer functions as the first method. Now, however the calculated transfer functions are sent to a centralized controller which will determine optimal values for alfa and beta.

Centralized system identification

All data received by the sensors is directly sent to a centralized controller which will calculate the transfer functions between all elements. This centralized controller will then configure each decentralized controller

4.2 Excitation signals

The selection of a suitable excitation signal is an important step in the design of an identification system [34]. There are different signal patterns possible each has its own advantages and disadvantages. In the past, the most common method to measure transfer functions was a combination of a slowly swept sine and a tracking filter (consisting of a series of single sine measurements at the desired frequency). Nowadays, more advanced digital signal processing algorithms are used. These algorithms use the fast Fourier transform to analyse the response. This makes it possibly to use more complex input signals. Instead of exciting the system frequency by

frequency, refined waveforms with a broadband spectrum are generated. These waveforms collect all spectral information in just a single measurement.

4.2.1 Measurement time

Before the transfer function of the system can be measured, the system has to reach its steady state. Every time the source signal changes it takes some time before the response is stable and periodic again. This initial situation is often called the transient state or the warm-up period. In the transient state the response changes due to the different time delays of the transmission paths between the actuators and the sensors. Remember that there are multiple transmission paths between a single actuator and sensor (due to reflections in the system). In Figure 12, this situation is shown for the actual system. At t=0.5s a single actuator is turned on, producing a 200 Hz signal. After a waiting time TW the response is approximately stable. This waiting time is approximately 0.4 seconds; it is the same for all excitation frequencies.

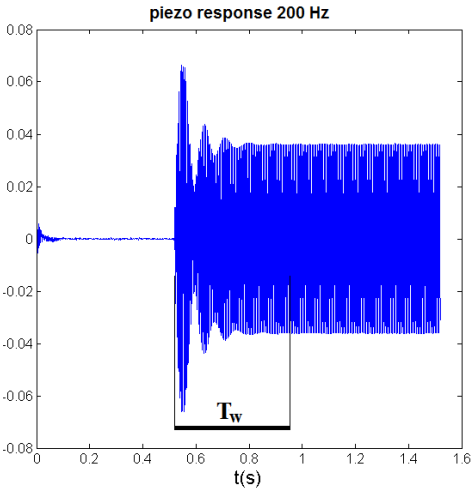

Figure 12 Wait time of the double-panel structure.

The stepped sine method has to wait T_w seconds at each frequency before it can measure the response. For an accurate measurement only a few samples are required when for example a Goertzel algorithm is used (this algorithm does not need a complete period of a sine for accurate results). The measurement time of the stepped sine method can thus be expressed as:

$$T_{ss} = F(T_w + T_M) \quad \textbf{(81)}$$

where T_m and F denote the measurement time of a single sinusoid and the number of frequency steps.

A broadband excitation contains a single period in which all frequencies in a specified range are excited. This period is repeated so that a periodic signal is created. When there is a good SNR this method only has to measure a single period. This measurement contains information for all frequencies. This measurement can start after the transients have disappeared, thus after a waiting time T_w. The broadband measurement time is

$$T_{bs} = \frac{1}{\Delta f} + T_w \quad \textbf{(82)}$$

where Δf is the frequency resolution, one period of the broadband measurement equals $1/\Delta f$.

A broadband signal distributes its power over F frequencies, while a stepped sine measurement concentrates all its power on a single frequency. Thus, the SNR ratio is much higher for the stepped sine method. To compensate for this poor SNR often the average of multiple periods of broadband excitation is used.

4.2.2 Broadband excitation signals

In this section broadband excitation signals are examined. The goal of this section is to understand the basics of these methods and to determine which resources are required to generate them and what is needed to extract information from their response. Broadband excitation signals are discussed in more detail by Pintelon [34]. In this section, two deterministic signals are inspected and a general conclusion about random excitation signals is presented.

Periodic chirp

This is the most basic broadband excitation signal. In one period a sine is swept from its lowest to its highest frequency. This is repeated so that a periodic signal is created.

$$u(t) = Asin\big((at + b)t\big) \qquad 0 \leq t < T_0 \tag{83}$$

With T_0 the period, $a = \pi(k_2 - k_1)f_0$, $b = 2\pi k_1 f_0$, $f_0 = 1/T$. The lowest frequency in this equation is $k_1 f_0$ and the highest $k_2 f_0$.

A periodic chirp can be generated by a single frequency controlled oscillator. This component is already present in the original setup. From the response all frequency components must be extracted by a FFT operation.

Schroeder multisine

The Schroeder divides it power in all frequencies equal. This broadband excitation signals is created by adding all frequency component together. This is shown in the equation below

$$u(t) = \sum_{k=1}^{F} Acos(2\pi f_k t + \varphi_k) \tag{84}$$

with Schroeder phase $\varphi_k = -k(k-1)\pi/F$.

This signal has a perfect spectrum, it excites only frequencies within the aimed frequency band. In Figure 13, this spectrum is compared with the spectrum of the periodic chirp method. In this figure the aimed frequency band had a lower limit of 2 Hz and an upper limit of 42 Hz.

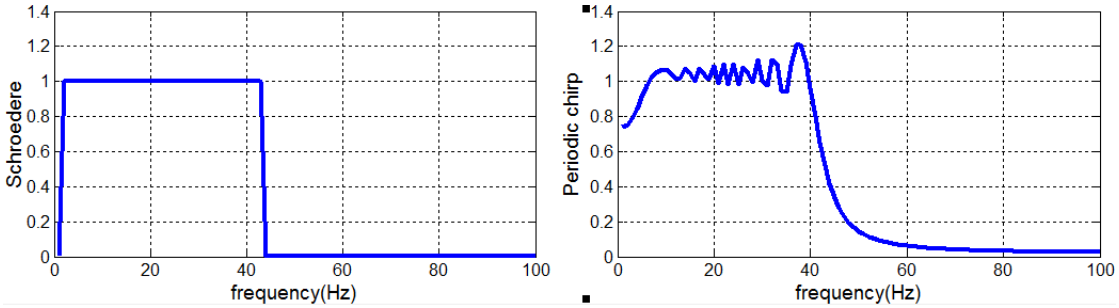

Figure 13 Broadband excitation signals in the frequency domain.

The main problem of the Schroeder multisine method is that it requires a FFT technique to generate the signal. This is too complex to implement it decentralized. For the analysis of the response also a FFT operation is required.

Random excitations

The mayor difference compared with periodic excitations is the variation in excitation from one realisation to the other. A random signal is transmitted by the actuator and received by the sensor. To extract the frequency response the original signal is required. This means that this method cannot be implemented decentralized. The original signal is only known at its source.

Deterministic excitations also have superior properties compared with random excitations. Random excitations putt less power in the system and are prone to leakage errors.

4.3 Conclusion

The preferred method for system identification is the decentralized implementation. In experiments the performance of such a system must be compared with a system which calculates the control effort weighting factor and the convergence rate centralized (see section 3.2). If the performance degration of the decentralized controller under normal circumstances is not very huge this method will be used. Else one of the other two methods should be chosen. Decentralized data processing might reduce the requirements on the data transport between the decentralized controllers and the centralized controller. Therefor as an alternative this method is chosen.

The extra hardware required for analysing and producing the excitation signals must be as little as possible. Hence, the best method is the simple stepped sine excitation signal. All hardware for this method is already present on the decentralized controllers. To accelerate this process a few frequencies can be analysed in parallel, similar to the Schroeder multisine method

5 Simulations

The simulations in this chapter use models of the transfer functions from a finite element model of the experimental setup. With this model the transfer functions between all actuators and sensors for frequencies from 10 to 1000 Hz were calculated. This includes the transfer function from the primary source to the sensors on the double-panel structure. All these transfer functions are an estimate of the true behaviour. Feedback control was also integrated in this model. So that the transfer functions with feedback could be obtained as well.

This chapter contains two sections. In the first section the control effort weighting factor for a decentralized controller is calculated for the entire frequency range. The resulting effort weighting factor will show if a decentralized implementation in the double-panel structure is realisable. In the second section a decentralized feedforward control system is created. This system will also contain a model of the plant, so that the performance of the controller can be analysed.

5.1 Control effort weighting

In this simulation the minimum control effort weighting factor β for the experimental setup is determined for the entire frequency range. In Chapter 3, two methods were presented to calculate the control effort weighting factor. The first method is an optimal solution based on the eigenvalues of the Hessian matrix of the cost function (see section 3.3). The second method uses Gersgorin's theorem (see section 3.5). This method is not optimal but easier to implement in a decentralized application.

The main goal of this section, is to determine if noise reduction can be realized by decentralized control of the double-panel structure. With equation (66) from section 3.6.2, shown below, this is analysed.

$$(\boldsymbol{E^H E})_{opt} = \sum_{m=1}^{L} \frac{\beta^2}{\lambda_m + \beta^2} |p_m|^2$$

If the system has a mode with an eigenvalue that in size is comparable to the effort weighting factor, then for this mode attenuation of the disturbance can be achieved. Therefore, in this analysis the largest eigenvalue is compared with the effort weighting factor.

Below, equation (47) from section 3.5.2 is shown. With this equation the effort weighting factor is determined according to Gersgorin's theorem.

$$|g_{ii}|^2 + \beta \geq \sum_{\substack{j=1 \\ j \neq i}}^{M} |g_{ii}^* g_{ij}|, \quad for\ all\ i$$

The ratio of $|g_{ii}|^2$ to β is determines if Gersgorin's theorem can make an accurate estimate of the eigenvalue. If beta is much larger than the square of the direct coupling than this theorem is not very useful.

First a configuration which only controls the radiant panel is examined. Then a system using both panels is analyzed and as last the effect of feedback is shown.

Controlling the radiant panel

With the data from the finite element model the values for $\beta_{Gersgorin}$, $\beta_{eigenvalue}$, $|g_{ii}|^2$ and λ_{max} are derived for all frequencies. In Figure 14, these parameters for the decentralized controller positioned in the middle of the radiant panel are shown. In this simulation, only the actuators on the radiant panel are controlled. For frequencies until approximately 320 Hz no control effort weighting is required (eigenvalue method). Thus, all modes of the disturbance signal can be suppressed in this region. From 320 to 400 Hz no attenuation is possible, all eigenvalues are negative in this region. At higher frequencies some results may be obtained especially in the 400 to 500 Hz range.

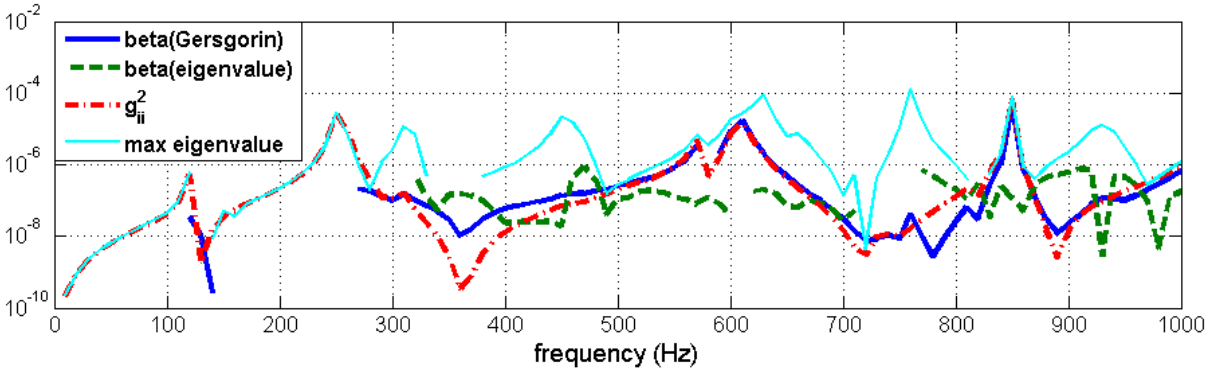

Figure 14 Simulation results of actuator sensor pair 1.

The beta determined by the eigenvalues of the Hessian matrix is lower for most frequencies than the beta of Gersgorin's method. However for some frequencies with Gersgorin's method a lower value for beta is obtained, this is because Gersgorin's method calculates for each decentralized controller a separate value for beta. A lower beta at a single decentralized controller will result in higher values for beta at the other decentralized controllers. Hence, the overall performance of the eigenvalue method is better. In Figure 15, the simulation results for another decentralizd controller are shown, to demonstrate this effect. For frequencies between 300 and 400 Hz the effort weighting factor is now higher for Gersgorin's method.

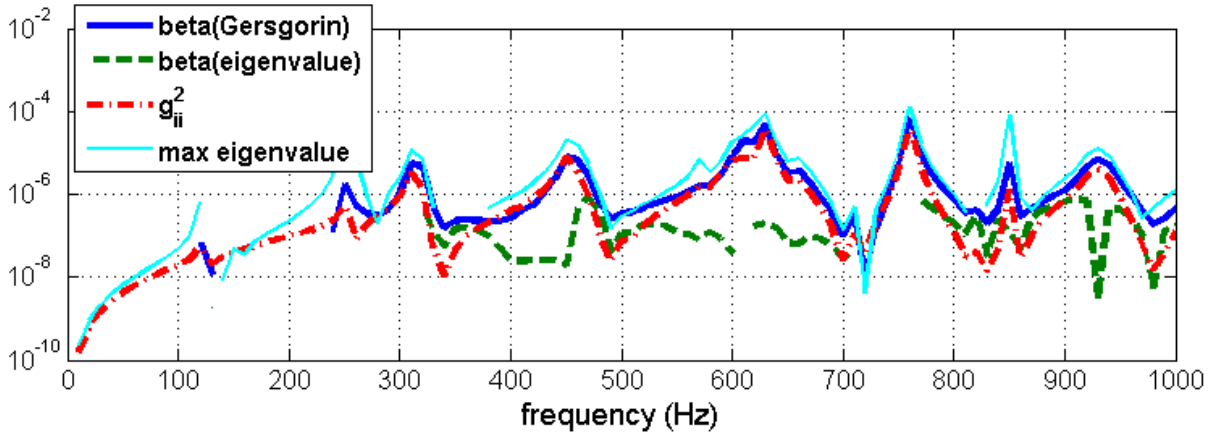

Figure 15 Simulation results of actuator sensor pair 2.

In the next experiment the direct-coupling and the cross-coupling of the decentralized controllers is examined. In Figure 16, the normalized power received by the centre acceleration sensor of the radiant panel is shown. This power is transmitted by the five actuators of the radiant panel. No control effort weighting is required if the cross-coupling of the system is smaller than the direct coupling. Thus, R1 must be larger than a half. The frequency regions that require no effort weighting correspond to the regions shown in Figure 15.

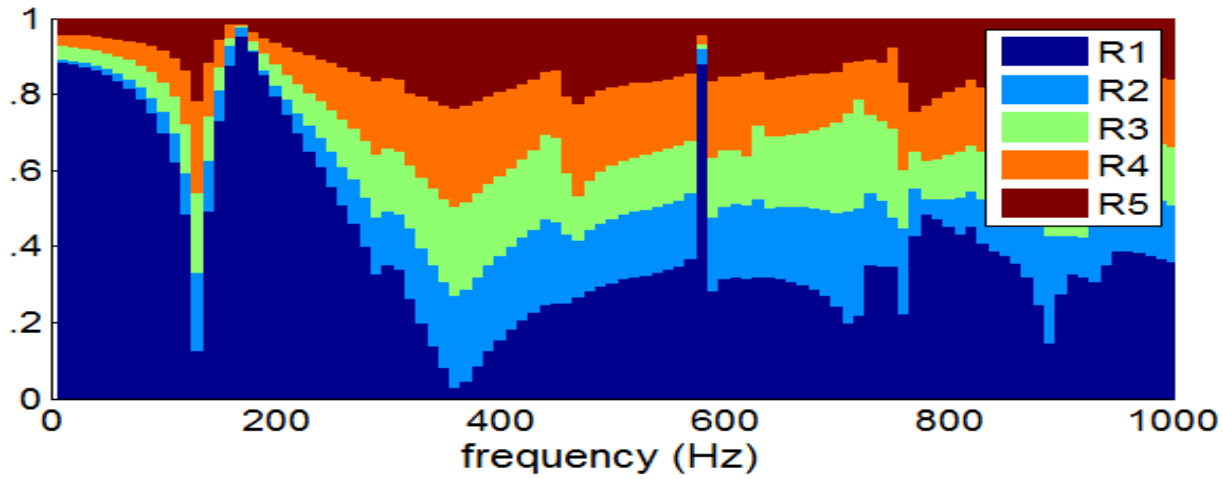

Figure 16 Actuator sensor pair 1: Direct coupling versus cross coupling.

Controlling both panels

If the decentralized controllers of both panels are used there is more cross coupling. Each sensor receives a signal from all sources. Which makes the overall contribution of the own actuator smaller. In Figure 17, the normalised received power of the centre sensor of the radiant panel is shown. At low frequencies the cross-coupling between the two panels is significant. At higher frequencies only the actuator in the middle of the incident panel has a significant contribution to the cross-coupling.

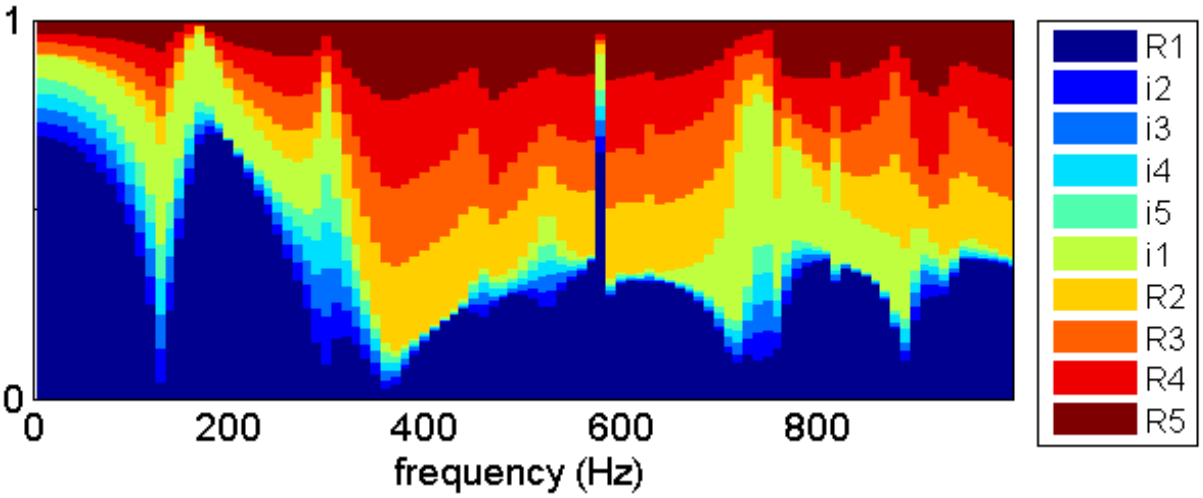

Figure 17 Actuator sensor pair 1: Direct coupling versus cross coupling both panels.

Controlling the radiant panel with feedback

In Figure 18 beta is determined for the decentralized control in the middle of the radiant panel with feedback. The feedback reduces the direct coupling, the values of $|g_{ii}|^2$ are smaller. For large regions the ratio β(eigenvalue) to max eigenvalue is smaller with feedback. However, there are some frequency ranges where the hessian matrix contains no positive eigenvalues, in this regions almost no noise attenuation can be obtained.

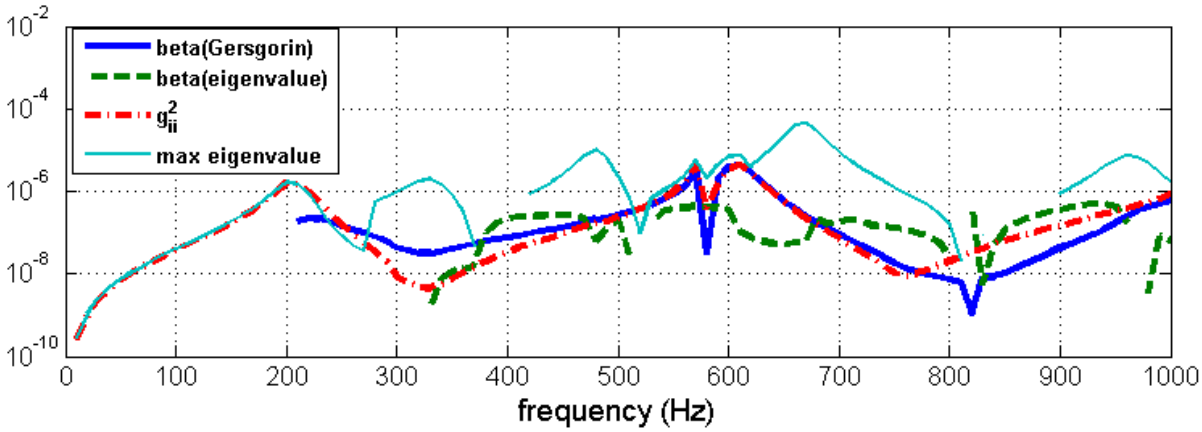

Figure 18 Simulation results with feedback of actuator sensor pair 1.

In Figure 19 the direct coupling and cross coupling are shown for the decentralized controller with feedback. The power distribution is much smoother; this makes it easier to estimate the entire spectrum. For the estimation of the spectrum, only a limited number of frequencies are measured. Between those frequencies an interpolation technique is used to estimate the response at the other frequencies. Hence, a smoother distribution requires a smaller amount of measured frequency components to estimate the entire spectrum.

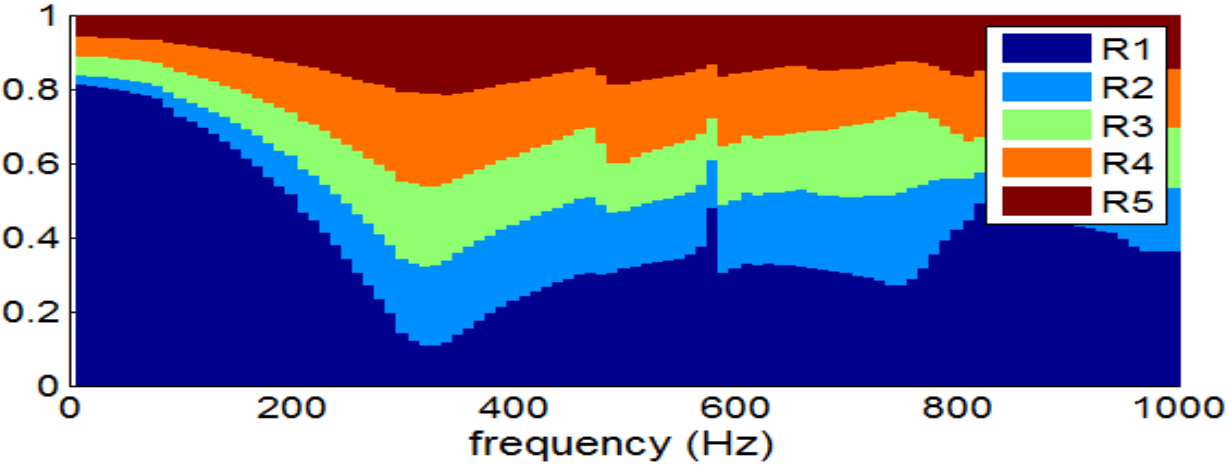

Figure 19 Actuator sensor pair 1: Direct coupling versus cross coupling with feedback.

Conclusion

With decentralized control the noise transmission of the double-panel structure can be reduced. All decentralized controllers interfere, and the more active actuators the larger the mutual disturbance. Controlling only the radiant panel requires the smallest control effort weighting factor. Feedback decreases the ratio β to largest eigenvalue, thus it might improve the overall noise reduction.

5.2 Adaptive decentralized Harmonic controller

In this section a model of an adaptive decentralized harmonic controller is developed in Simulink. This controller operates on each harmonic separately. For every harmonic a different configuration is required. With this model the theoretical performance of the controller is studied.

In Figure 20, the top level model of the simulation setup is shown. The plant and the controllers are created in the frequency domain, thus no time to frequency domain transformations are required.

The disturbance signal has a constant value. In this model it is assumed that there are no time delays.

The plant is transformed to the principal component form (see section 3.6), hence the behaviour of all modes of the plant can be examined. The model contains two controllers; with a manual switch you can select the desired controller. The Principle component controller is added to demonstrate that specific principal components can be supressed without influencing the other principal components. The decentralized harmonic controller is the real test controller which will be used in the normal configuration. Also notice the “turn control on” block, this block will turn the controller on after half a second. The first half second the disturbance signal is not suppressed.

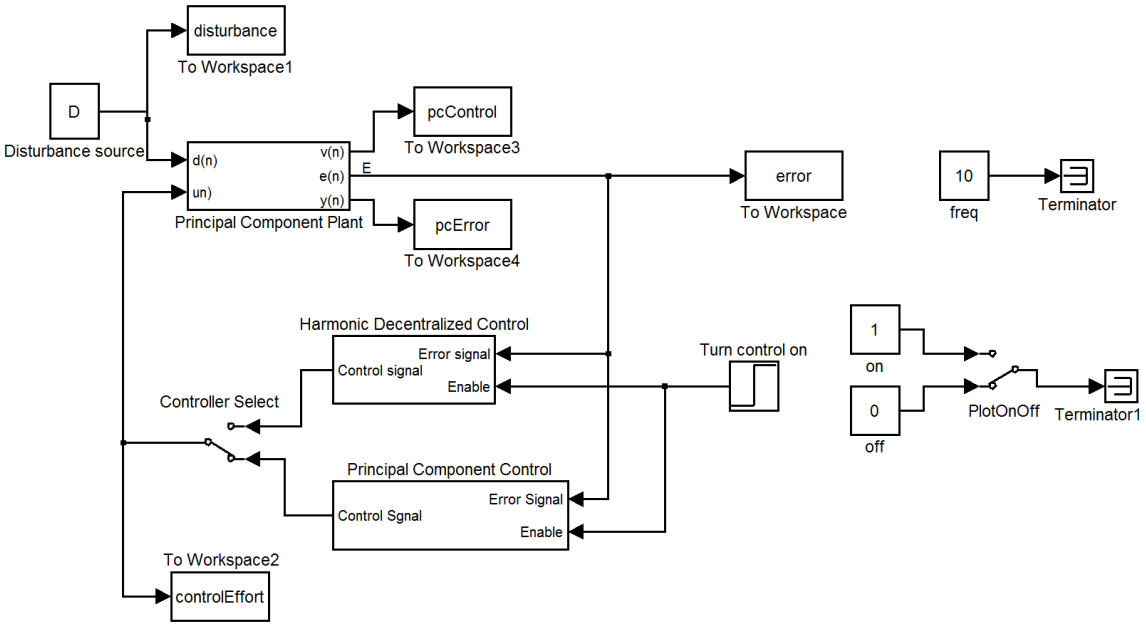

Figure 20 Top level presentation of the model.

When this Simulink model is opened it will call a Matlab function which will load the transfer function data from an external file. From this date the gain matrixes of the model are derived for all possible frequencies. Also the minimum control effort weighting factor for a stable decentralized system is calculated for all frequencies (the equations of chapter 3 are used).

However, the model operates only at a single frequency. In the “freq” block diagram this frequency can be specified. Every time when a new simulation is started, a Matlab function is called which will initialise the blocks of the Simulink model. The frequency dependent blocks point to matrixes in the Matlab workspace. This data is adjusted for the correct frequency. The values used for the control effort weighting parameter and the convergence rate are specified in this function, as well.

Harmonic decentralized controller

The decentralized harmonic controller uses the following equation to update the control signal. The initial control signal is equal to zero.

$$\boldsymbol{u}(n+1) = (1-\alpha\beta)\boldsymbol{u}(n) - \alpha\widehat{\boldsymbol{G}}^{H}\boldsymbol{e}(n)$$

In this equation $\hat{\mathbf{G}}$ is the estimated plant transfer matrix which contains only the direct coupling

elements. Thus, all non-diagonal components are zero. In Figure 21 the block diagram representation of this control law is shown. The values of α and β are derived from the Hessian matrix of the cost function (see section 3.3). Furthermore, the minimum value of β is limited to one thousandth of the maximum value of β (β has a different value for each frequency). An enable signal is added to this model, it can reset the initial state of the control signal and can deactivate the controller. The controller is active when the enable signal is high; else it will output a value equal to zero.

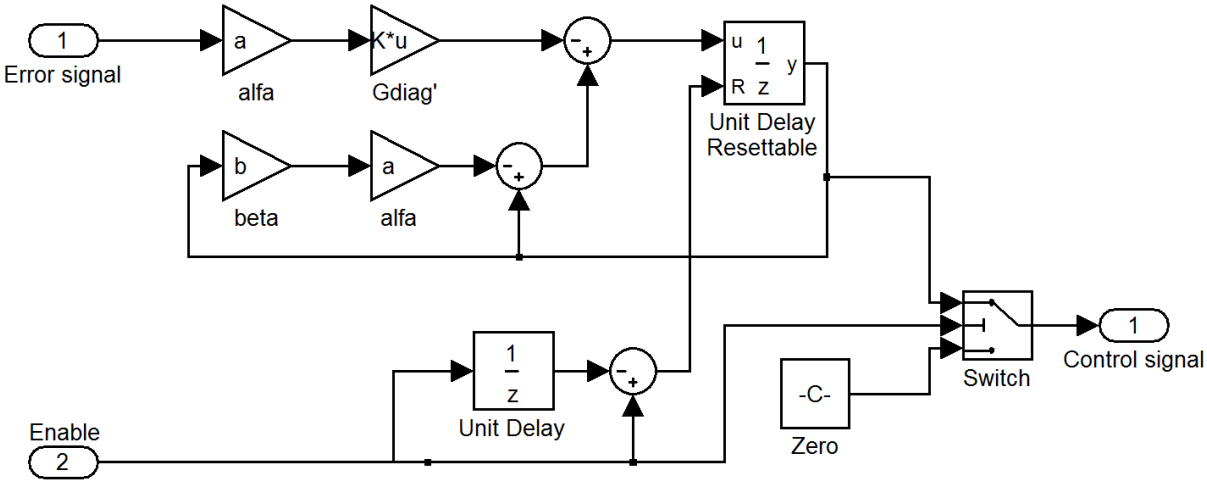

Figure 21 Decentralized adaptive controller with control effort weighting.

For the Harmonic Decentralized controller different datasets can be selected. These datasets contain the transfer functions from the complex plant and from the disturbance source to the plant. Each dataset has a different feedback configuration of the plant (also no feedback). Furthermore, the feedforward configuration can be selected.

In this simulation multiple configurations are simulated and their results are compared. For each configuration the behaviour between 10 – 1000 Hz is analysed. Each simulation had a length of 5000 steps. In this amount of steps, the algorithm could converge to its optimal solution for all frequencies. The best indication of the transmitted sound by the panel is by looking at the kinetic energy of the radiant panel (see section 2.3). However, in this simulation the mean square acceleration of the panel is measured. The mean square velocity of the panel is proportional to the kinetic energy of the panel. The magnitude of velocity is equal to the magnitude of the acceleration divided by the angular frequency, $v = {}^{a}/_{\omega}$. The mean square acceleration is thus almost proportional to the kinetic energy of the panel.

The following three configurations are examined:

Pressure speaker feedback combined with radiant panel feedforward

In the future, six pressure speakers will be installed in the cavity of the double-panel structure. In Figure 22 the mean square acceleration of the radiant panel is shown for different control strategies. The previous section showed that low frequencies require no control effort weighting. This simulation shows that indeed the best performance is obtained in this region. All resonance peaks below 400 Hz of the system are removed by the feedback and feedforward combination. The

feedforward controller on its own can not remove the peak near 130 Hz. The resonance frequency of the acrylic box is 420 Hz, the peak in the frequency response at this frequency can not be removed.

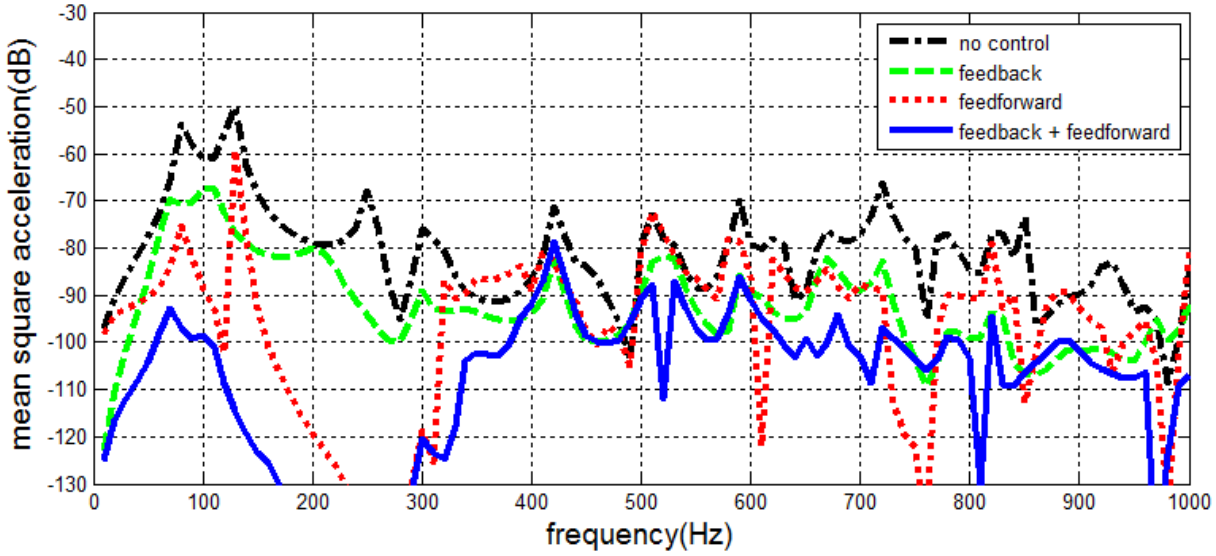

Figure 22 Mean square acceleration of the radiant panel with pressure speaker feedback and radiant panel feedforward control.

In Figure 23, the summed control effort of all actuators on the radiant panel is shown. The control effort signal is compared with the magnitude of the disturbance signal. In this figure only the control effort of the feedforward algorithm is shown, the feedback algorithm requires additional control effort. Both configurations require the most control effort at low frequencies. The addition of feedback reduces the amount of control effort that is required.

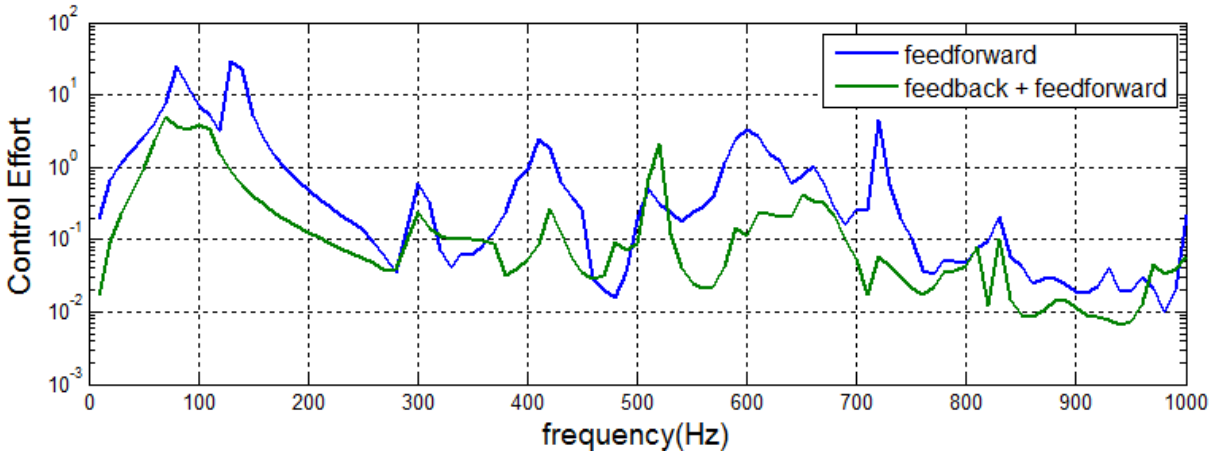

Figure 23 Control effort of the radiant panel.

For all frequencies the adaptive algorithm converges to its optimal solution. Figure 24 shows how many steps were required to reach this optimal steady-state. This state is reached as soon as the algorithm stays within a 1% deviation range of its final state.

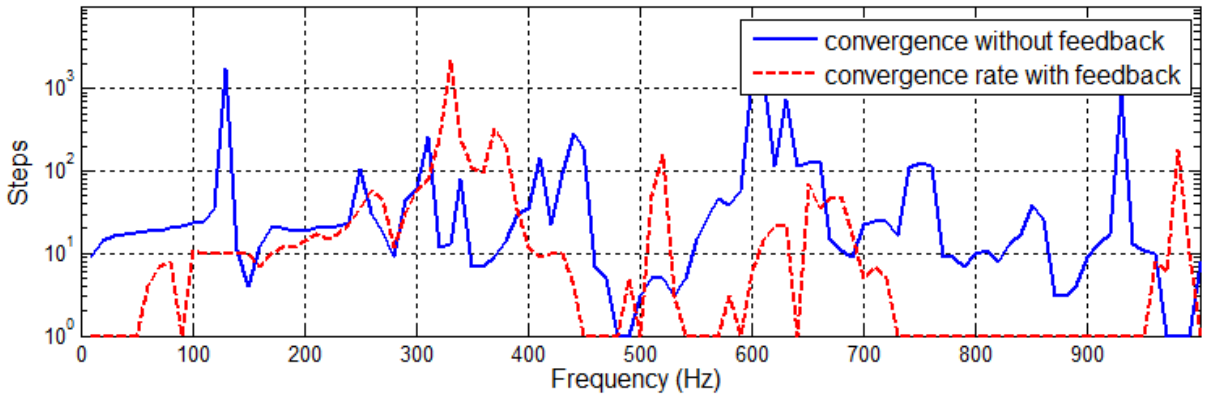

Figure 24 Convergence rate of the two configurations.

Radiant panel feedback combined with radiant panel feedforward

The same experiment is performed for a configuration with feedback from the radiant panel instead of the pressure speakers. This feedback configuration can only achieve little noise reduction on its own, as you can see in Figure 25. However, in combination with feedforward control some significant reductions can be obtained. Compared with the previous configuration, at high frequencies more reduction is achieved. At lower frequencies this configuration performs less well. The resonance peak near 130 Hz can not be removed. The required control effort and the convergence rate of this configuration are similar to the previous configuration.

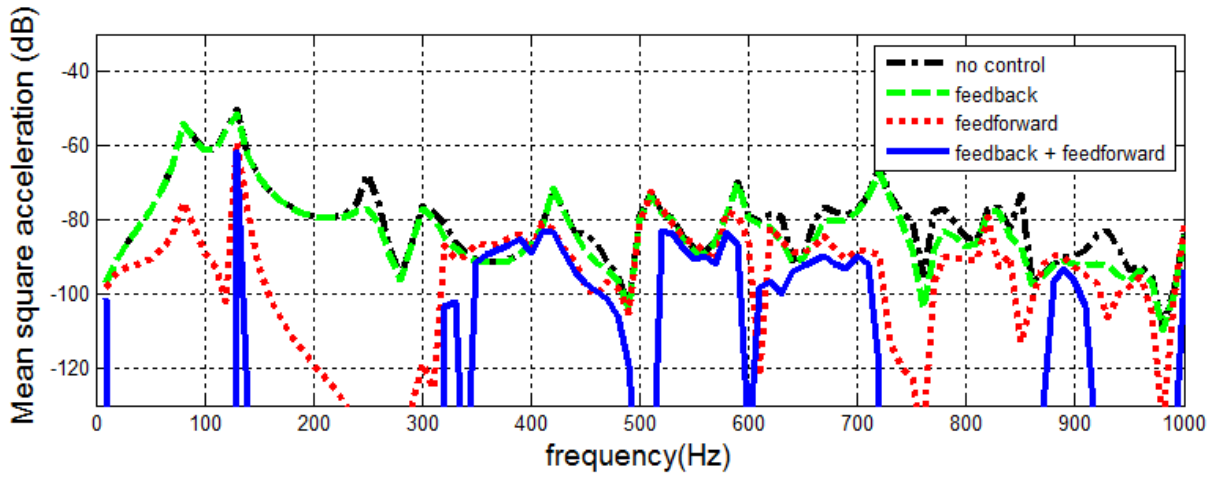

Figure 25 Mean square acceleration of the radiant panel with radiant panel feedback and radiant panel feedforward control.

Pressure speaker feedback with both panel feedforward

In Figure 26 the simulation results for this configuration are shown. The feedforward control is able to reduce the first two resonance frequencies by 20 dB. This is much more than the feedforward control of the radiant panel could achieve. At higher frequencies its performance is worse. The addition of feedback does not improve the noise reduction by much.

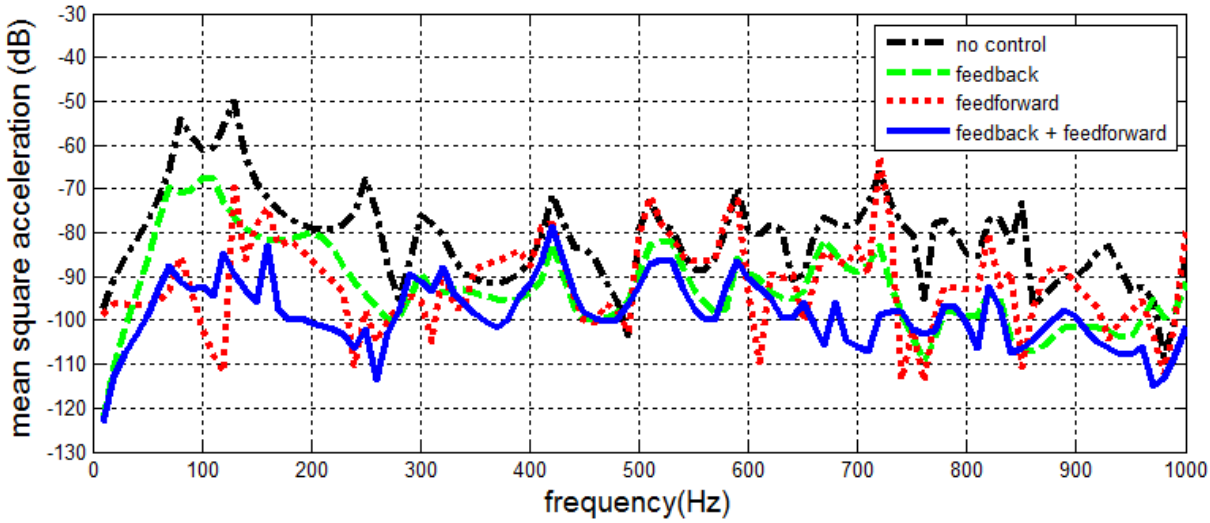

Figure 26 Mean square acceleration of the radiant panel with pressure speaker feedback and radiant + incident panel feedforward control.

In Figure 27 the control effort of the incident panel is shown. For low frequencies these control efforts are very high, approximately 2 to 3 times higher than the control effort of the radiant panel. Inserting such large control signals in the system may result in unstable behaviour.

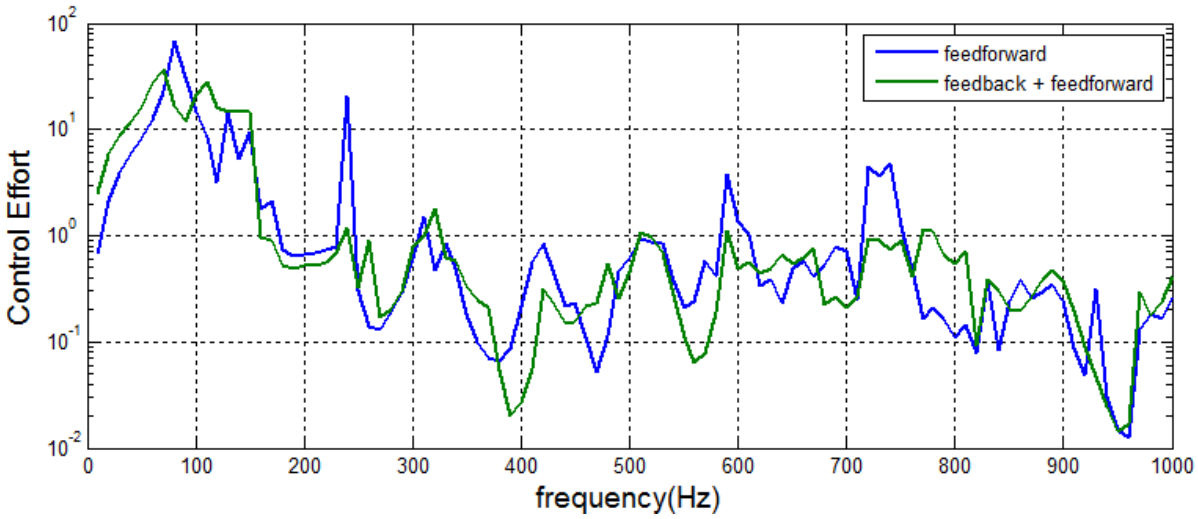

Figure 27 Control effort of the incident panel.

6 Implementation

In this chapter self-created C MEX S-functions and complete Simulink models are explained. The C MEX S-functions are used in Simulink to perform small tasks; they are used in the complete models.

Simulink models for system identification and decentralized feedforward control are treated in this chapter. From basic models more complex models are derived which will perform their task faster or with less resource. All implementations in this chapter are used on the real setup, no offline analysis models are presented here. All blocks work in the real-time mode of Simulink, in the real-time mode no complex output signals are allowed.

Simulink has a large library of blocks which all perform a specific function. Most of these blocks are written in C MEX S-functions, this are C/C++ functions which have specified methods which are called by the Simulink engine. They are written in C/C++ for faster execution. In Simulink all these blocks are connected, and the execution order is determined. The fewer blocks your model contains, the faster the execution is. In this paragraph the behaviour of the created blocks is explained. All created blocks can handle a dynamical number of inputs. So that they can be used to control a dynamical number of actuator sensor pairs without any modifications

6.1 Stepped sine system identification

In Figure 28 the stepped sine system identification diagram is shown. This system controls a single actuator and it measures the error signals of all sensors of the double-panel structure. The system identification model is connected to the plant, which is shown in this diagram as well. In reality, the plant is not inside the model and it should be replaced by AD and DA converter blocks with their corresponding filters.

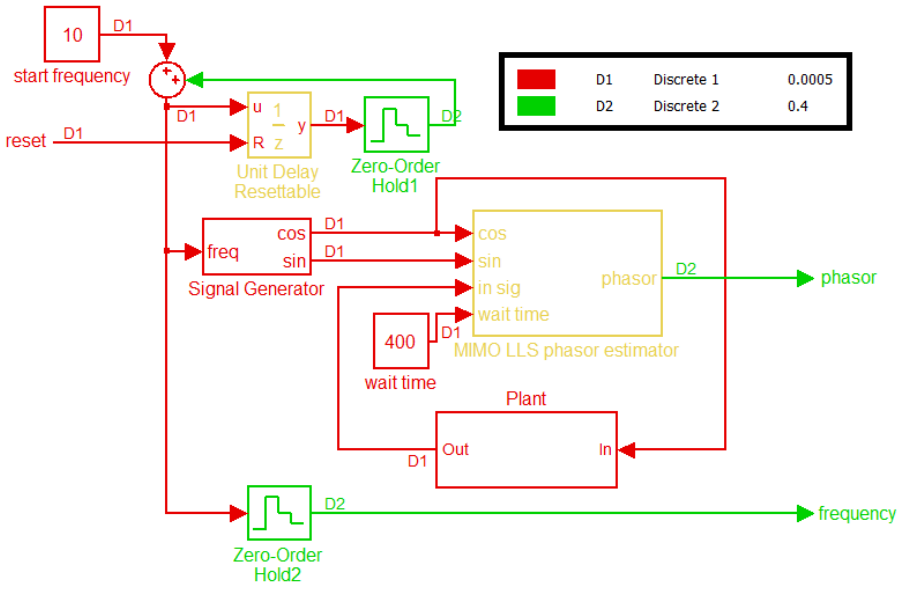

Figure 28 Stepped sine system identification.

The stepped sine model contains some logic to generate the stepped sine wave and a LLS phasor detector. For all blocks the sample rates are shown. Every 0.4 seconds the frequency is increased with 10 hertz. The identification process will end as soon as the frequency reaches 1000 Hz. After a frequency change the system waits 400 samples before the response is measured. In this time the transients of the system can disappear, so that a steady-state response is measured (see section 4.2.1). The following 400 samples are used for a linear least square estimation of the phasor of the error signals (see section 3.8.3). In Figure 29 a timeline of this process is shown, the numbers on the horizontal axis are the sample times.

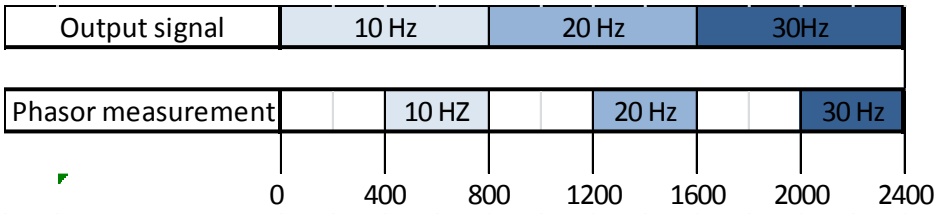

Figure 29 Input and output signals of the system identification model.

The presented system identification model estimates for all sensors the frequency response of a single actuator. For a complete identification of the plant, this model must be executed for each actuator. The double-panel structure contains 5 piezoelectric actuators on both panels, hence the total time required for measuring all the transfer functions of the double-panel structure is

$$T_m(s) = (5+5) \cdot (0.4s \cdot 100) = 400s$$

6.2 System identification parallel

In Figure 30, the parallel stepped sine system identification model is shown. This model measures the transfer function from one actuator to all sensors. For a complete system identification this process must be repeated for all actuators.

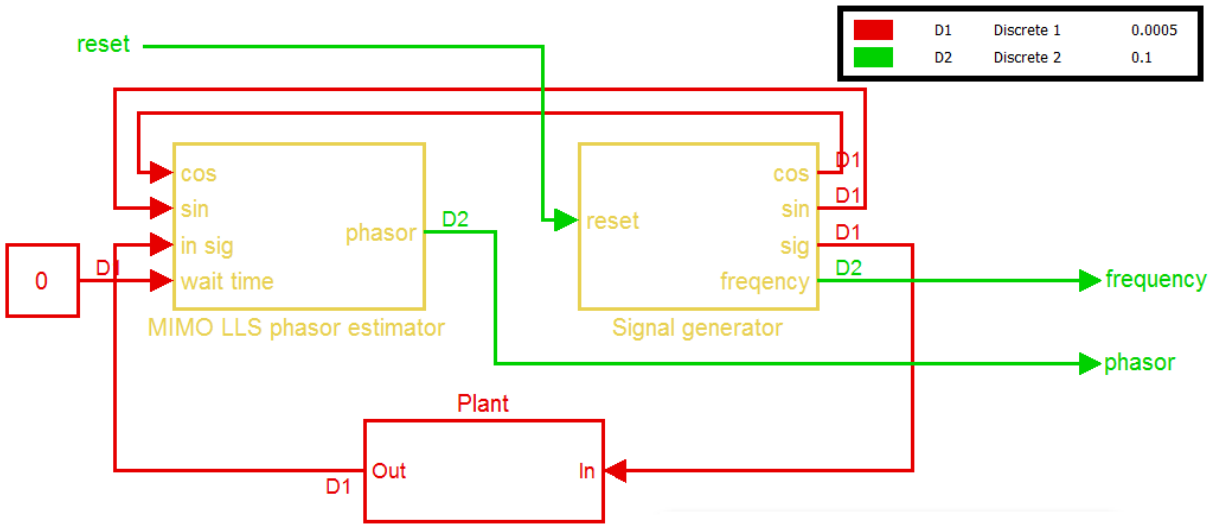

Figure 30 Parallel System identification model.

In Figure 31 the timeline of the execution of this model is shown for the first samples. The transmitted signal by the signal generates consists always of four frequency components. Every 0.1 seconds a frequency component is removed and a new one is added. In the simple stepped sine method of the previous section the LLS phasor estimate block was only working half the time. Every time it had to wait till the transmitted signal became stable again, before it could start a new measurement. In this model the LLS phasor estimate block is working continuously. In 200 samples the phase and amplitude of a single frequency component is measured.

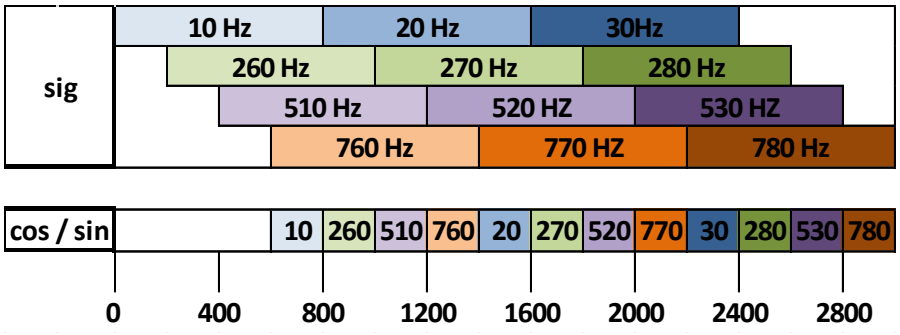

Figure 31 The output signals of the signal generator block.

6.3 Decentralized feedforward controller

In Figure 32 the scheme of the adaptive decentralized feedforward controller is shown. In the previous section the AD DA blocks were not shown, however in this scheme they are. The three blocks that form the controller are shown in the centre of the figure. The MIMO LLS phasor estimator block is used in the system identification part as well, this block measures the error signals. The green block is the feedforward controller, it determines the control signals from the error signals. The last block of the controller generates the time domain control signals. Furthermore, it generates the reverence signals for the LLS phasor estimator. The blue blocks in the diagram can be accessed and updated during the execution of the model. The blue blocks on the right store the measured signals and with the blue blocks on the left the frequency can be selected and several components can be activated or deactivated. Besides the controller also the disturbance signal is produced in this model. All input and output signals have a sample rate of 2000 Hz. The adaptation process has a frequency of 2.5 Hz.

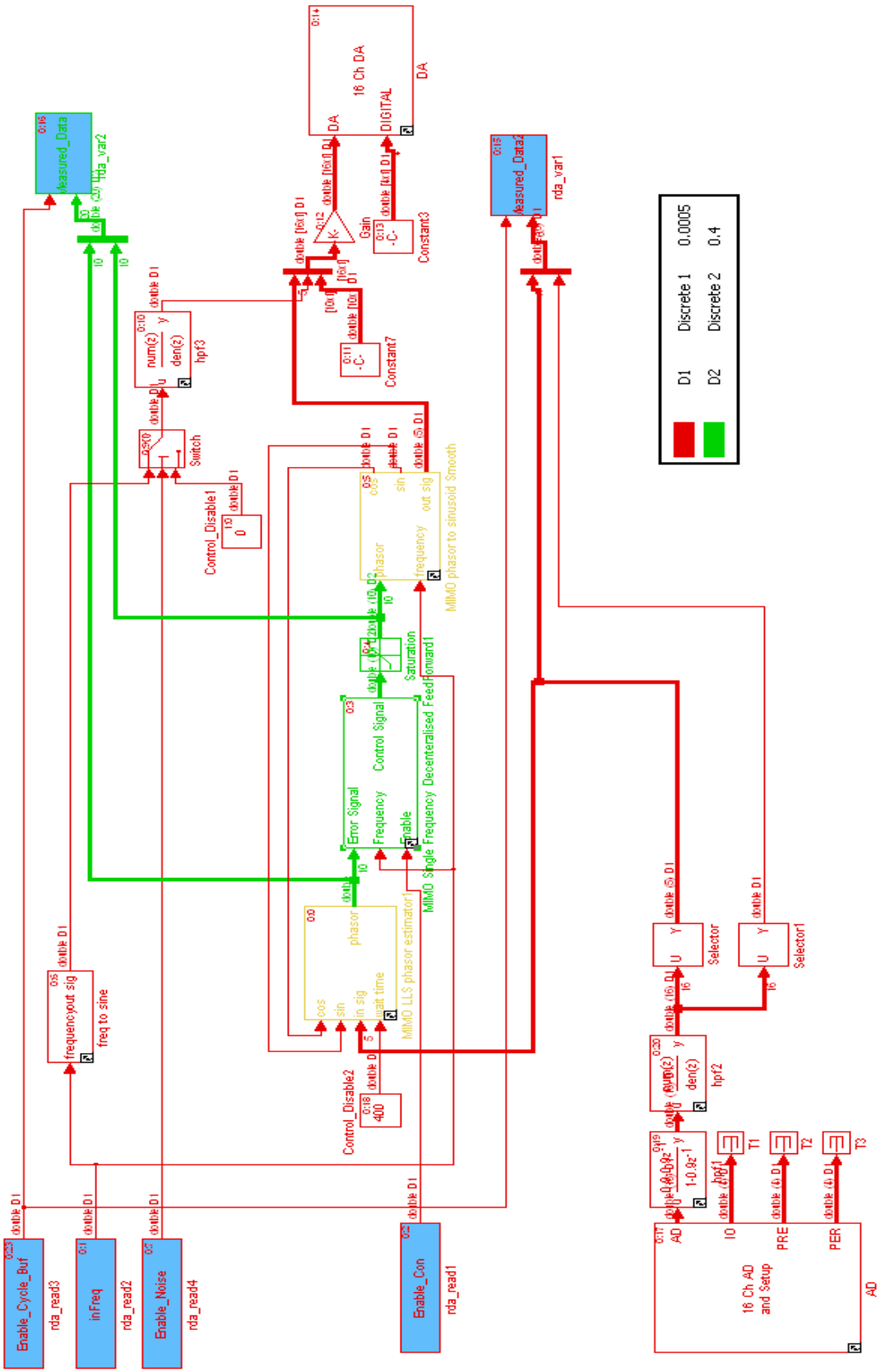

Figure 32 The decentralized adaptive feedforward controller.

The MIMO single frequency decentralized feedforward controller is the crucial block of this scheme. This block calculates the control signals for multiple actuator sensor pairs, no information is exchanged between pairs. So it is a real decentralized feedforward controller.

The input 'Error Signal' is a phasor which is split into a real and imaginary component. This input can receive a dynamic amount of error phasors. The 'Error Signal' has the following format:

$$\boldsymbol{e} = \begin{bmatrix} Re\{A_1 e^{i\theta_1}\} \\ Im\{A_1 e^{i\theta_1}\} \\ \cdot \\ Re\{A_n e^{i\theta_n}\} \\ Im\{A_n e^{i\theta_n}\} \end{bmatrix}$$

The block diagram has three important parameters, **α**, **β** and **G**. These parameters must be specified before a simulation is started. Parameter **G** has the following format:

$$\boldsymbol{G} = \begin{bmatrix} Re(G_{f(1),e(1)}) & Im(G_{f(1),e(1)}) & \cdot & Re(G_{f(1),e(n)}) & Im(G_{f(1),e(n)}) \\ \cdot & \cdot & \cdot & \cdot & \cdot \\ Re(G_{f(n),e(1)}) & Im(G_{f(n),e(1)}) & \cdot & Re(G_{f(n),e(n)}) & Im(G_{f(n),e(n)}) \end{bmatrix}$$

The width of matrix G must be equal to the size of vector **e.** The parameters **α** and **β** are specified in a similar way. For each error signal at each frequency a value for these parameters is specified. However, these parameters are not complex, so they are not split into two components.

Linear interpolation

The input 'frequency' determines which values of the tables are used, Linear interpolation is used to fill the gaps between the table elements. The controller will react on changes of the disturbance frequency. At each iteration the output 'control signal' is updated. Equation (37) is used to calculate the control signal.

7 Experiments

In this chapter the experimental setup is introduced and its behaviour is analysed. This analysis will show if harmonic control with piezoelectric actuators is possible. The implementations from the previous chapter are tested in practise. Their results are compared with the results in the simulations. Furthermore, the effect of varying circumstances on the harmonic decentralized feedforward controller is examined.

7.1 The experimental setup

The fuselage wall of an airplane contains an inner wall and an outer wall. Between these two walls a cavity is present which can contain some materials. On the inner wall the noise reduction system will be mounted. Of this wall an experimental setup is created which has similar resonance frequencies.

In Figure 33a the experimental setup is shown. An acrylic box with 40 mm thick walls is mounted on top of a structure which contains a large speaker. This speaker produces the primary disturbance signals. The 40 mm thick walls will transmit almost no sound, all sound is pertained in the box and can only escape through the double-panel structure which is mounted on top of the acrylic box (and

through the structure of the speaker). Through reflections of the top and bottom of the acrylic box resonance frequency will occur, which have wavelengths similar to the dimensions of the box.

The incident panel of the double-panel structure is made of aluminium and the radiant panel has a honeycomb structure. Between these two panels is a 35 mm air gap. In the table below all the dimensions and the densities of the double-panel structure are shown.

	Parameters	Value	Unit
Acrylic box	inner dimensions wall thickness	420 ·297 · 350 40	mm^3 mm
Aluminium panel	dimensions density	420 ·297 · 2 2700	mm^3 kg/m^3
Middle cavity	dimensions	420 · 297 · 35	mm^3
Honeycomb panel	dimensions density	420 · 297 · 5.8 409	mm^3 kg/m^3

In Figure 33b the radiant panel is shown, on this panel five piezoelectric actuators are mounted. These actuators are controlled independently and can control the panel at different resonance modes. On top of actuators accelerometers are put. With five accelerometers on one panel an accurate estimate of the kinetic energy of the panel can be made till about 1000 Hz. On the aluminium panel the same configuration of sensors and actuators is installed. All sensors and actuators are installed on the upper side of the panels.

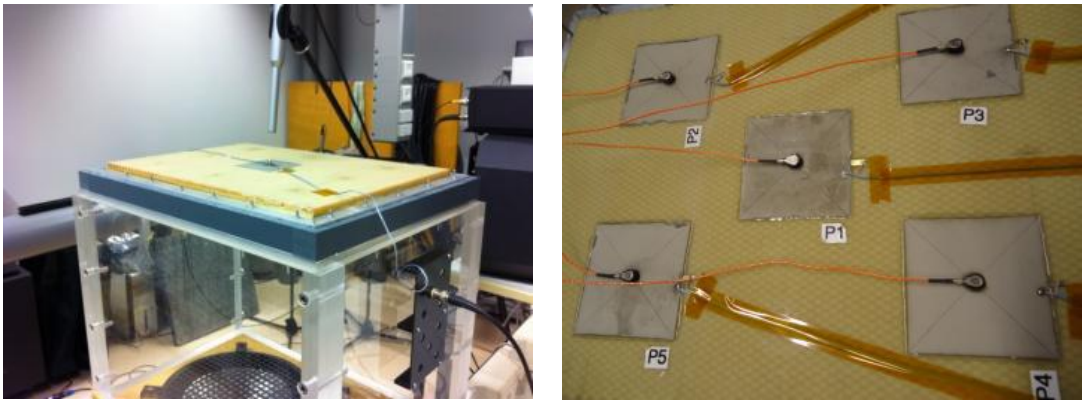

Figure 33 a) the experimental setup, b) the radiant panel.

7.2 Measurement system

In the current development phase all actuators and sensors are connected to a Linux platform. On this platform all outputs and inputs can be controlled with real-time models created in Simulink. These models have a sample time of 2 kHz. However, the signals send to the actuators are up sampled to 100 kHz.

In the next phase of the development of this noise reduction system the collocated actuators and sensors will have their own processing unit. For decentralized feedforward control no connection with an external platform is required anymore, everything is processed locally. However, during the system identification phase still some connectivity with a centralized controlled is required to coordinate this process. Thus, not all wires on the panel can be removed.

The next section will specify the components used to measure signals in the current system. Also the behaviour of the platform is tested. With this information all measured signals can be transformed to real acoustic quantities.

Accelerometer

Accelerometer: Deltaron accelerometer Type 4517-002
Sensitivity: 1.0 mV/ms^{-2}
frequency range 1Hz to 20 kHz (amplitude +-10%)

This input signal is amplified with a factor 10 by the sensor signal conditioner before it is send to the tar-r1-xenomai.

Microphone

Sensitivity: 515 mV/Pa
This is the sensitivity including all amplifiers. For the measurement a device was used which produced a 1 kHz signal with a sound pressure level of 94 dB (this is 1 Pascal).

Platform

Input gain tar-r1-xenomai: 0.037
Output gain tar-r1-xenomai: 12.34

The output signal of the platform is filtered by a low-pass and a high-pass filter. The low-pass filter is used to remove the DC-component and the high-pass filter is an anti-alliasing filter.To test the response of the system, the followinge experiment is performed. In a simulink model a sinusodial signal with an amplitdude of 0.1 volt is generated. This output signal is directly coupled to the input of the platform and measured again by the same simulink model. In Figure 34, the measured frequency response is shown. On an analog scope the same signal was measured, it had a simular shape as the signal shown in the figure below. Thus, the main transformation of the signal occurs at the output stage in the DA conversion.

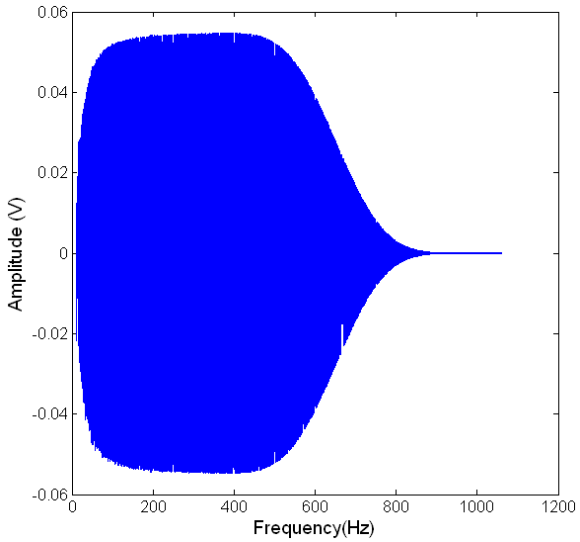

Figure 34 Frequency response of the platform.

7.3 Frequency response analysis

In this section, the frequency response of a collocated actuator sensor pair is examined. For the control algorithm it is important that the signal produced by the piezoelectric actuators have low harmonic distortion and other distortions. Each controller can control the disturbances only at its tuned frequency. So, all signals at other frequencies are uncontrolled and produce undesired sound. This will degrade the performance of the control system.

In Figure 35, the transfer function of an actuator sensor pair is shown. The experimental setup only contained a single panel during this test, so the resonance peaks in the response differ from results shown elsewhere in this report.

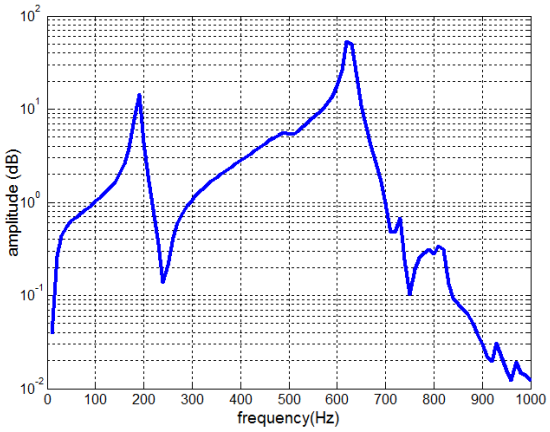

Figure 35 Transfer function of an actuator sensor pair of a single panel structure.

In Figure 36, the complete output spectrum for each input frequency is shown. The actuator transmits a signal with the frequency shown on the “input frequency” axis. As input signal a slowly swept sine was used (see section 4.2). After measuring 800 samples, the frequency of the sine is increased with 10 Hz. The first 400 samples of the measured signal are ignored, because it takes some time to reach a steady state after there has been a frequency change. A fast Fourier transformation is performed on the last 400 samples. The measured output spectrum is scaled; the frequency bin of to the input signal is set to one.

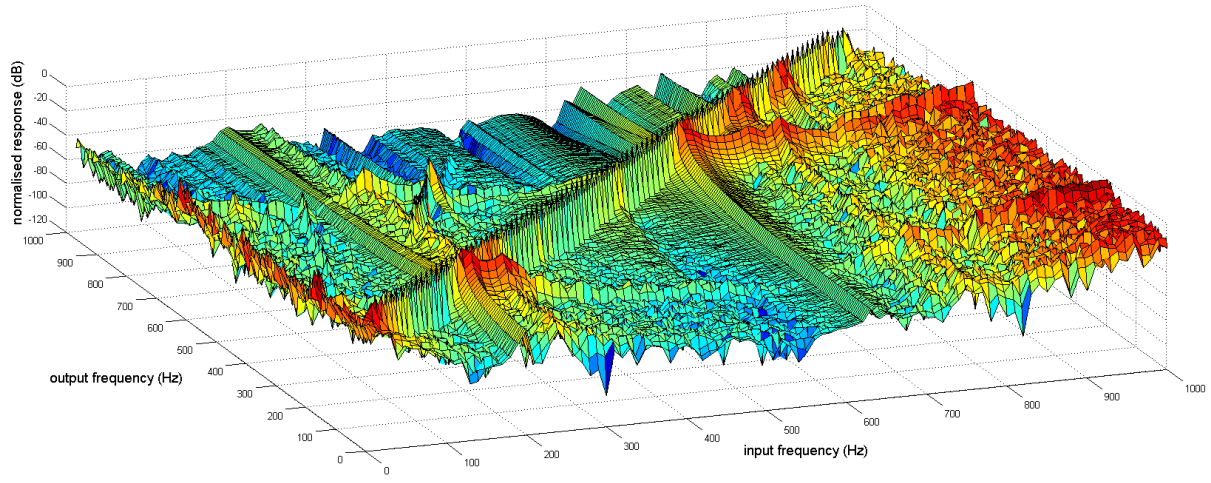

Figure 36 Normalised frequency response of an actuator sensor pair.

The largest measured frequency component is equal to the fundamental frequency for all input excitation frequencies. For low and high frequencies the measured spectrum is more broadband, this is due to the settings of the DA converter which attenuates these frequencies (see Figure 34). The first harmonic is good visible around 300 Hertz. Higher harmonics are not excited much. Even after normalisation the distortion is still larger at the resonance frequencies of the system than at other frequencies. All frequencies also excite the resonance frequencies, for all input frequencies there is a small response visible at approximately 190 and 630 Hz. When the actuator is controlled with a sinusoid of 630 Hz all other frequencies are also excited relatively more.

7.4 Transient state inspection

At each iteration of the adaptive algorithm the control signals change. In one sample time, Δt, the phase and the amplitude are modified to the new derived values. Due to this abrupt change in amplitude and phase the system needs time to reach its steady state again. In Figure 37, the response of a single error sensor during the feedforward adaptation process is shown. Each time the control signal is updated a peak in the response appears. This non steady state limits the speed of the convergence rate. After each update of the control signal you have to wait till the transients of the system disappear before the new steady state error can be measured.

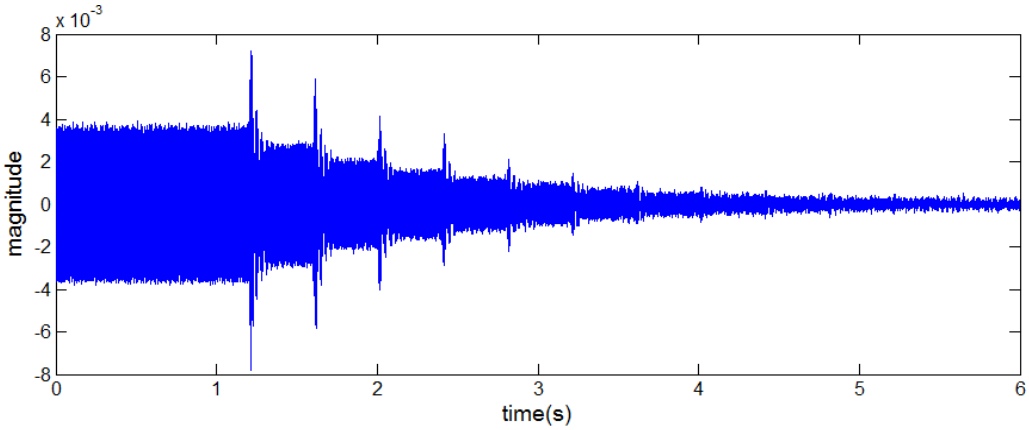

Figure 37 Response of a single sensor during the feedforward adaptation process.

In this paragraph the response during the transient state is examined. This response is compared with responses of less abrupt changes in the control signal. If the control signal update excites other harmonics, the performance of the controller might be limited. Also when there is no leakage to other harmonics during the control signal update process, it may for example be possible to control and measure other frequencies during the current transient state.

The rapid modification in the phasor results in a large change of the response of the system. Smoother transitions might have a positive effect on the response. In this paragraph a smooth transition will be compared with an abrupt modification of the phasor. In the equation below, a linear transition of the control signal is shown:

$$u(t) = \begin{cases} A_1 cos(\omega t + \varphi_1) & t \le t_0 \\ \left(1 - \frac{t - t_0}{t_1 - t_0}\right) A_1 cos(\omega t + \varphi_1) + \frac{t - t_0}{t_1 - t_0} A_2 cos(\omega t + \varphi_2) & t_0 < t \le t_1 \\ A_2 cos(\omega t + \varphi_2) & t > t_1 \end{cases} \quad \textbf{(85)}$$

In Figure 38, for three different speeds of modification the time and frequency domain behavior during a control signal change are shown. At $t=t_0=0.05s$ the control signal is changed, its phase is shifted with 90 degrees and its amplitude is increased with a factor 2. The control signal will change between t_0 and t_1 linear to its new state. In

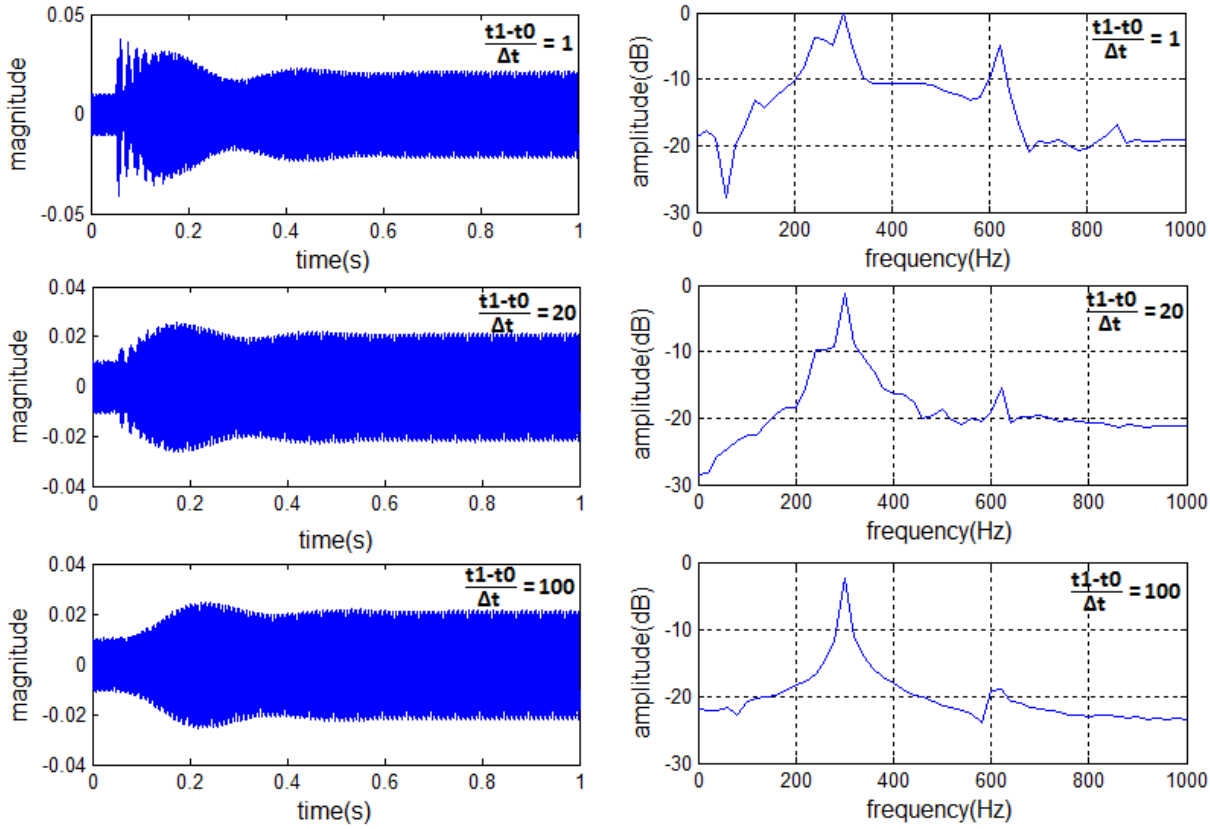

Figure 38 Control signal updates at three different rates. The left figures show the time response of the collocated acceleration sensor, at t=0.05s the control signal of the piezoelectric actuator is changed. The right figures show the frequency response during this update, the first 100 samples after the start of the updating process are used.

The slow linear transition between control signals removes the leakage to other frequency components significantly. The abrupt peaks in the time domain are removed. In the frequency domain the undesired peak close to 600 Hz is almost entirely removed.

However, the above mentioned method can not be integrated in the current system. The feedforward controller stores the amplitude and the angle of the signal which it is currently transmitting. A change in phasor as described by equation (85) can not be realized in the current implementation without changing the structure significant. Thus, another comparable method is used instead. This method changes the amplitude and angle of the old control signal linear in 100 steps to the new control signal. In Figure 39, this method is shown in action. The spikes during the control signal update process are removed.

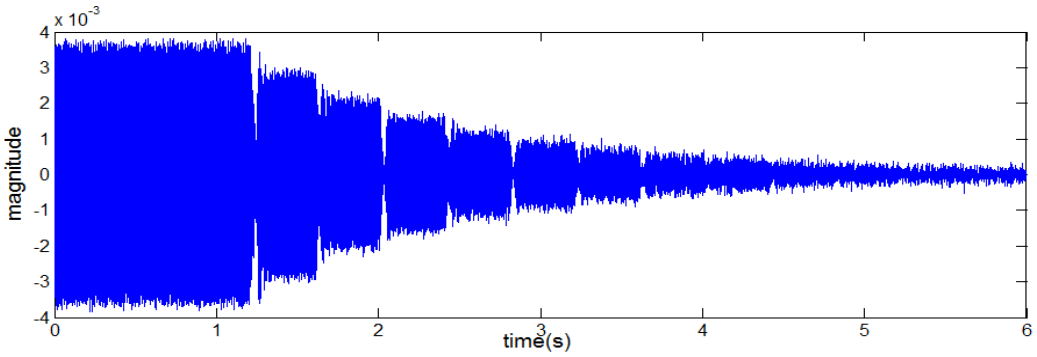

Figure 39 Response of a single sensor during the feedforward adaptation process with slow control signal updates.

In Figure 40 the Fourier transform of 200 samples direct after a control signal update is shown (blue solid line). The red dotted line is the old abrupt update method. The new method reduse he leakage to neighbouring frequencies and the excitation of other frequencies is reduced.

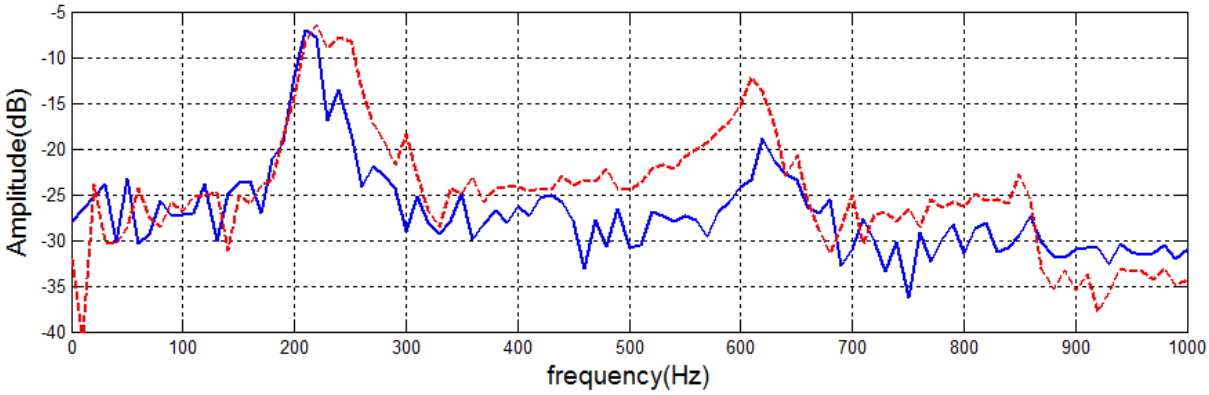

Figure 40 Frequency response of a single sensor just after an adaptation step during the feedforward adaptation process. The red dotted line is the old abrupt control signal modification technique and the blue solid line is the new slowly adjusting technique.

Conclusion

The control signal update technique presented in the section has several benefits over the old abrupt control signal update technique. The first advantage is that the abrupt peaks during a state transition are removed, these peaks produce undesired sound. As can be seen in Figure 40, the total power of the signal during the transition is reduced. Also the leakage to other frequency components is significantly reduced. Thus, it may be possible to control and measure other frequencies during the current transient state. This phenomenon is examined further in section 7.5.2**.**

7.5 System identification

In this section the accuracy of the system identification models presented in the implementation chapter are examined. First the results of the most simple algorithm, which uses the LLS phase estimation technique is compared with a reference method from which is known that it behaves appropriate. Next the accuracy of the more complex parallel frequency excitation system is analysed.

7.5.1 Verification of the stepped sine method

The amplitude measured by the implementation explained in section 4.2 is compared with an existing trusted setup. This operation is performed to verify the correctness of the developed

method. The other method uses a device called SigLab, this device performs 100 fast frequency sweeps (periodic chirp, see section 4.2.2). The duration of each frequency sweep is approximately 0.5 seconds. The results of all sweeps are averaged. The blue solid line in Figure 41 shows the amplitude response for the entire frequency range for this system. The LLS system identification method is shown in this figure as well. Between 100 and 600 Hz the two methods measure similar responses. At higher frequencies the results differ, this is due to the limited passband of the platform (see section 7.2).

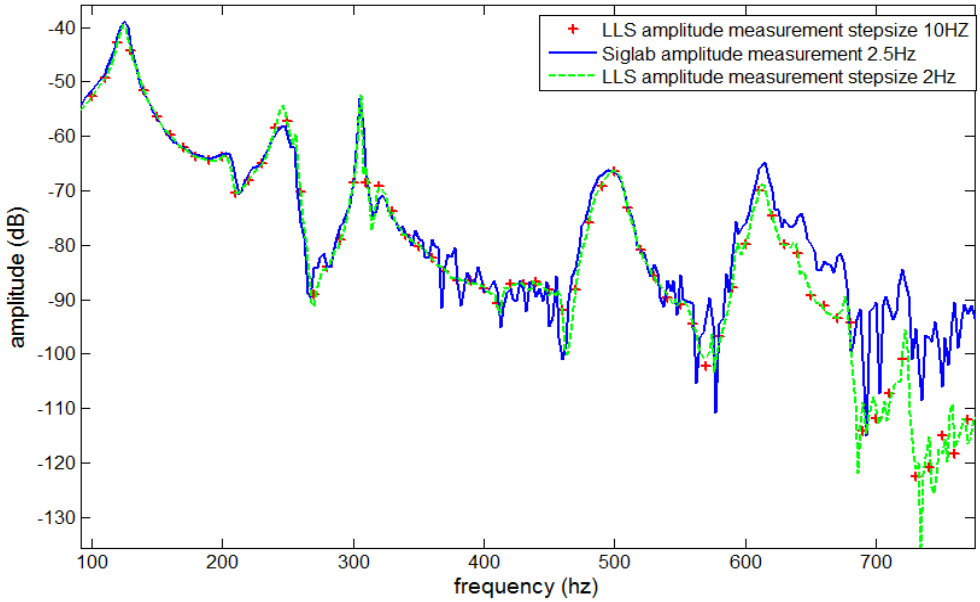

Figure 41 LLS amplitude estimation validation.

The stepped sine method is run with 2.5 Hz and 10 Hz frequency steps. The 10 Hz steps miss the resonance peak at 310 Hz. With linear interpolation the response at this frequency can not be estimated. This might result in an unstable system. Thus, the frequency step size of the stepped sine must be smaller than 10 Hz.

7.5.2 Parallel stepped sine method

In this section the performance of the parallel stepped sine method of section 6.2 is examined. The response of this method is compared with the response of the non-parallel method of the previous section. In Figure 42the magnitude response of both methods are shown. This is the response from a single actuator to its collocated sensor. The measured magnitudes of both methods are similar, only in regions where the response is very small some differences are noticeable.

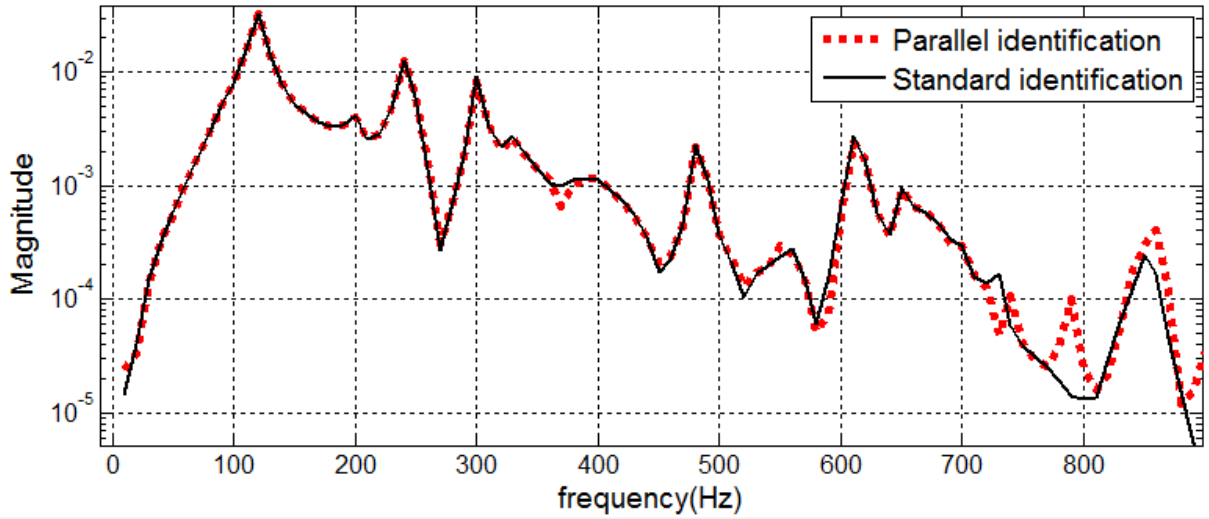

Figure 42 Magnitude response of parallel and standard system identification.

In Figure 43 the phase difference of both methods is shown. At the resonance frequencies the phase difference is small and at frequencies where the structure is only slightly excited larger phase differences are measured. For these slightly excited frequencies no control is required thus the parallel method for system identification can be used in the double-panel structure.

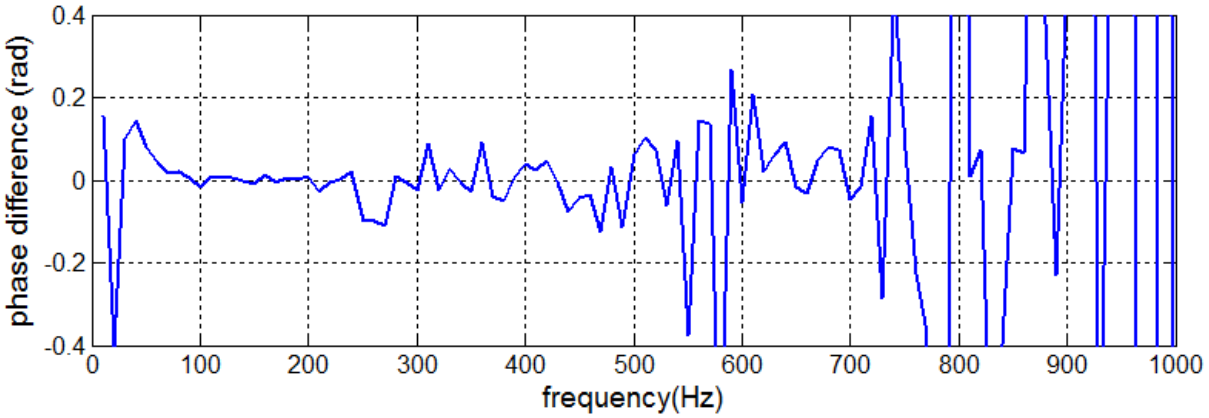

Figure 43 Phase difference of the two system identification methods

7.6 Offline analysis

In the simulations of Chapter 5 the complex plant response was estimated by a finite element model. In this section the frequency response of the experimental setup is used in an offline setup. This setup is shown in Figure 44, it contains an adaptive decentralized feedforward controller, a model of the plant and a disturbance source. Furthermore, there are a few blocks that record the error and control signals. Each colour in the model represents a sample rate. Yellow blocks have multiple sample rates. An exact copy of the decentralized feedforward controller is used in the real setup. In this section, the theoretical performance of the decentralized feedforward controller is examined. In the next section these results are compared with the true practical values.

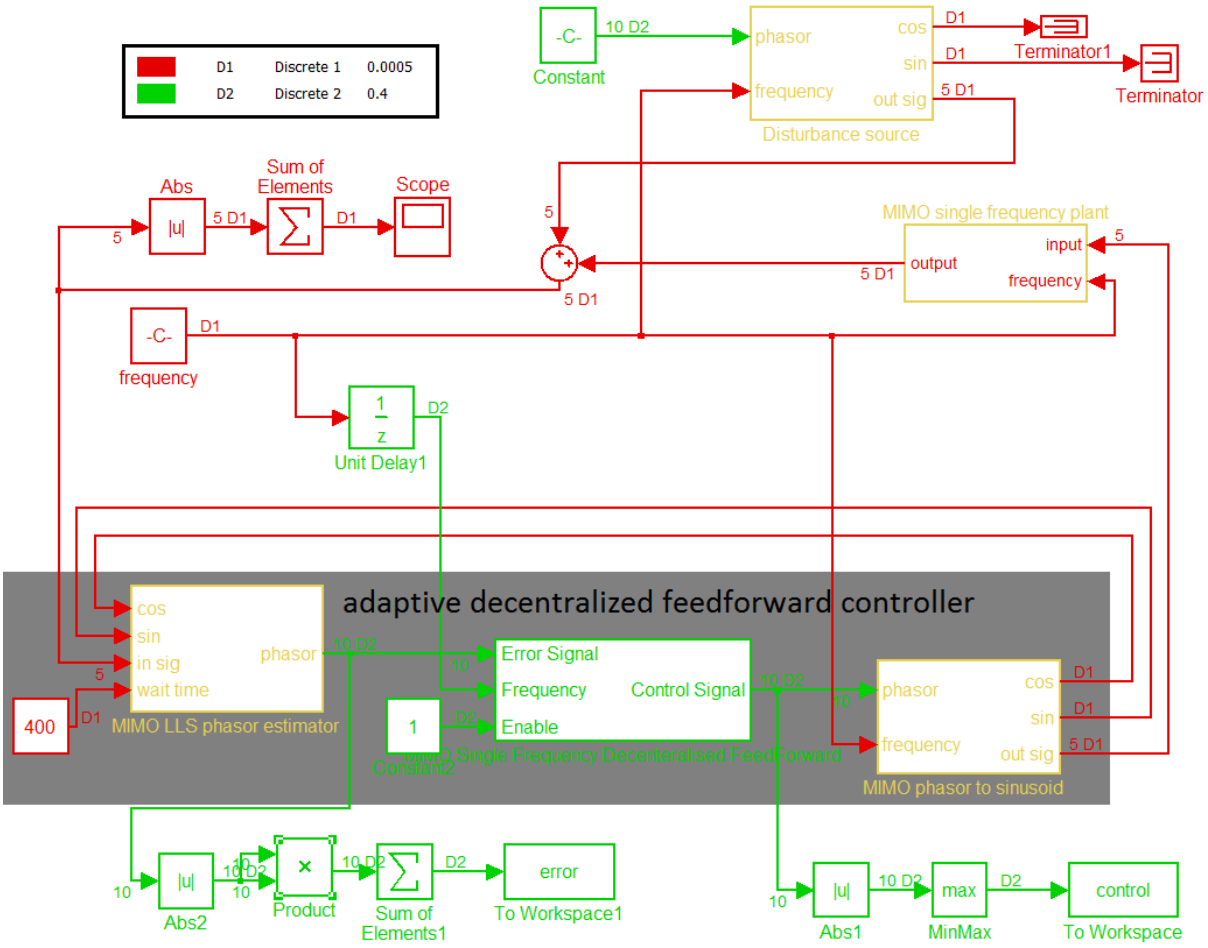

Figure 44 Offline model of the feedforward controller and the plant.

The decentralized controller is configured with two techniques. The first technique uses Gersgorin's theorem to determine the value of the control effort weighting factor and the second method sets the control effort weighting factor based on the eigenvalues of the Hessian matrix of the cost function. In Figure 45, the kinetic energy of the radiant panel for both control strategies is shown. Only the radiant panel is controlled in this simulation.

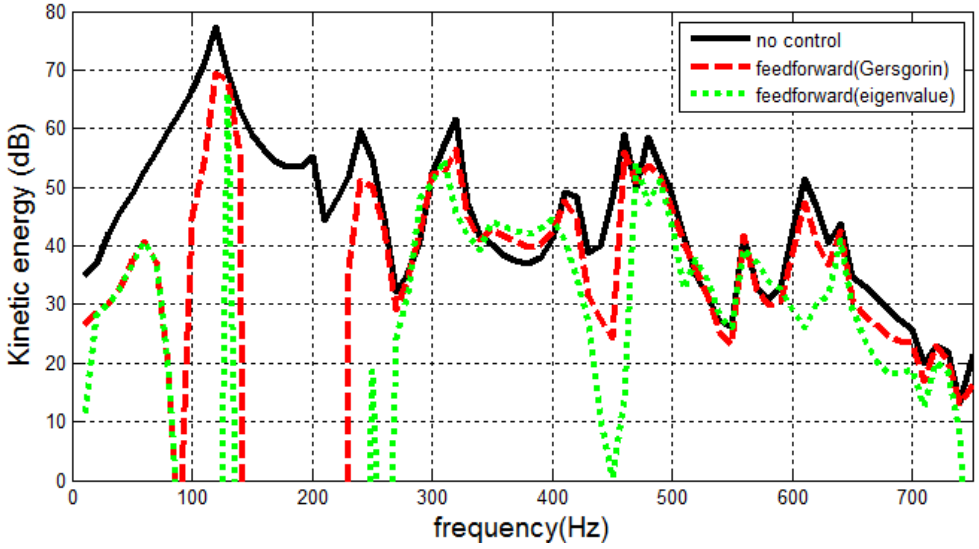

Figure 45 Kinetic energy radiant panel with offline decentralized feedforward control.

The performance of the configuration based on the Hessian matrix is better. However, the method based on Gersgorin's theorem, reduces the kinetic energy significant at low frequencies as well. In Figure 46 the maximum control effort of an actuator on the radiant panel is shown. This is the control effort required to the keep the structure in its steady state. At low frequencies the control effort of both methods is very similar. The control effort is small for all frequencies, the actuators on the real setup are able to produce control signals with this magnitude.

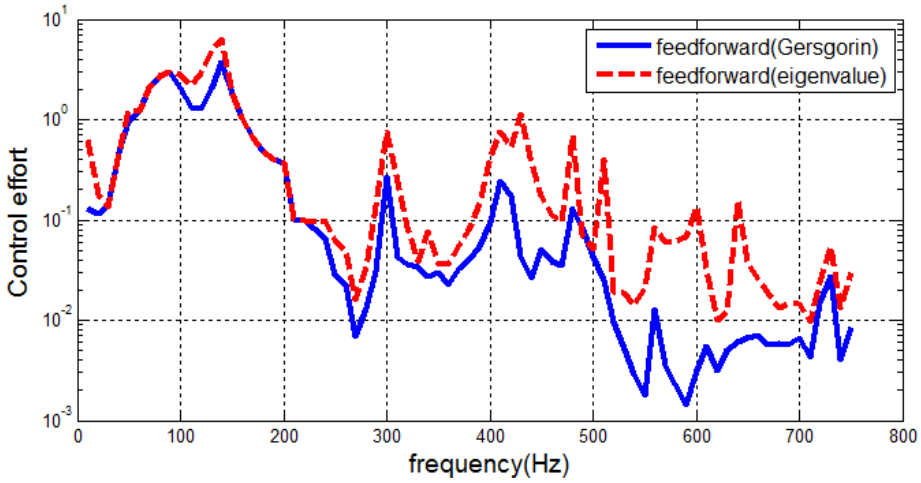

Figure 46 Steady-state control effort of the hardest working actuator.

Both methods obtain significant reduction in the kinetic energy of the double-panel structure. Therefore, the performance of both methods must be examined on the real setup.

7.7 Adaptive harmonic feedforward controller

In this section the performance of the feedforward algorithm on the real setup is analysed. In the first part of this section the performance of the algorithm based on the Hessian matrix of the cost function is analysed extensively. It is also compared with the simulations. In the last part of this section different control strategies of the panel are compared with each other. For all experiments the controller shown in section 6.3 is used.

The performance of the controllers is analysed by measuring the kinetic energy of the panel and the sound pressure level above the structure. The kinetic energy of the panel is approximated by the following equation

$$E_k \propto \frac{1}{N} 10 log_{10} \left[\sum_N \left(\frac{a_i / \omega}{v_{ref}} \right)^2 \right] \quad \textbf{(86)}$$

Where a_i is the amplitude of the acceleration measured by sensor i, N the number of sensors, ω is the angular frequency and v_{ref} is the reference velocity. The reference velocity is equal to $5.0 \cdot 10^{-8}$ m/s (see section 10). The calculated value is proportional to the kinetic energy.

Minimising the total kinetic energy of a structure does not generally result in the minimisation of radiated sound. In fact a reduction of vibration may be accomplished by an increase in sound radiation. Therefore, a microphone is placed 15 cm above the panel to measure the transmitted sound of the panel.

7.7.1 Configuration based on the Hessian matrix of the cost function

In Figure 47 the kinetic energy of the radiant panel is shown. At each frequency a disturbance signal is produced for 10 seconds. During the first second the controller is not activated, hence the disturbance is not suppressed. After one second the controller is activated and the control algorithm has 9 seconds to reduce the disturbance as much as possible. In the first second the noise without control is measured and in the last second the noise with control is measured.

The kinetic energy reduction in the simulation gives a good identification of the reduction on the real-setup. Only minor differences are observable. Still the simulation is a bit to optimistic.

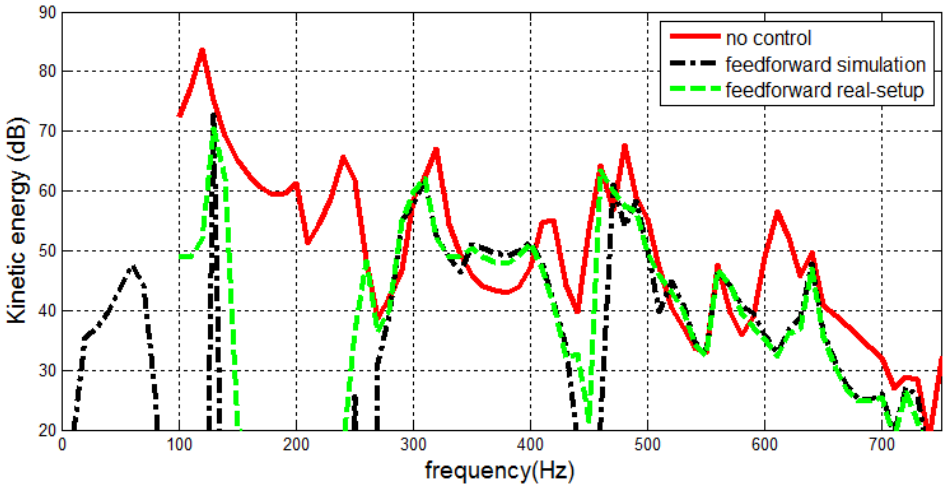

Figure 47 Kinetic energy of the radiant panel.

In Figure 48 the sound pressure level(SPL) measured by a microphone above the structure is shown. The background noise was 30dB. The SPL is not reduced as much as the kinetic energy. Below 300 Hz the reduction is proportional to the kinetic energy reduction. At 320 Hz the resonance frequency is even amplified. In the conference paper *Panel Resonance Control and Cavity Control in Double-Panel Structures for Active Noise Reduction* [35] it is shown that this resonance peak comes from the

radiating panel where all lower resonance frequency come from the incident panel. This might explain this difference but further investigation is required.

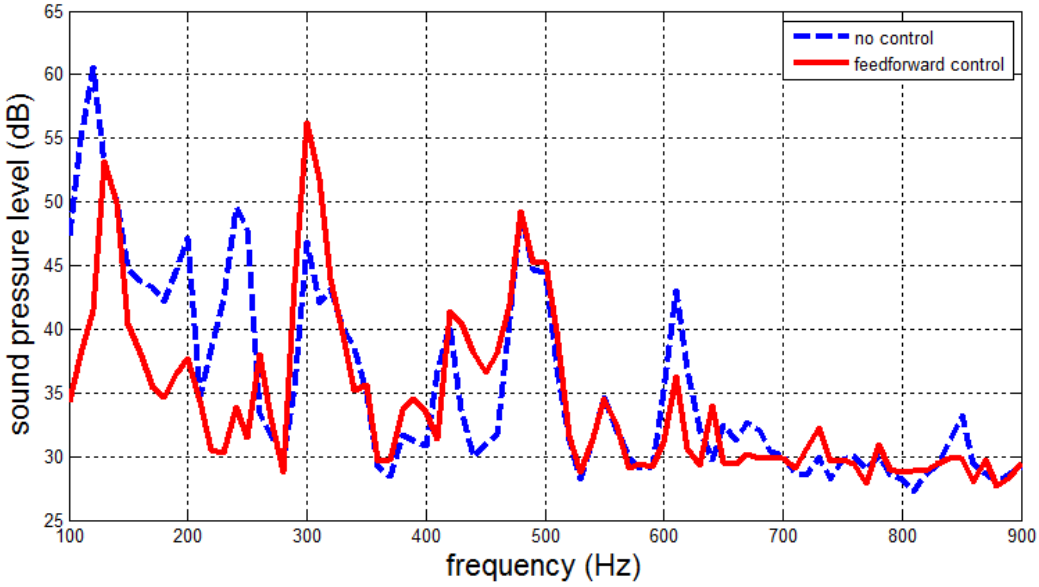

Figure 48 Sound pressure level above the panel.

The control effort in the simulation is compared with the control effort in the real setup, this is shown in Figure 49. In the real-setup the control effort is slightly higher, but no real large differences are observed. Except, at 780 Hz were the algorithm became unstable.

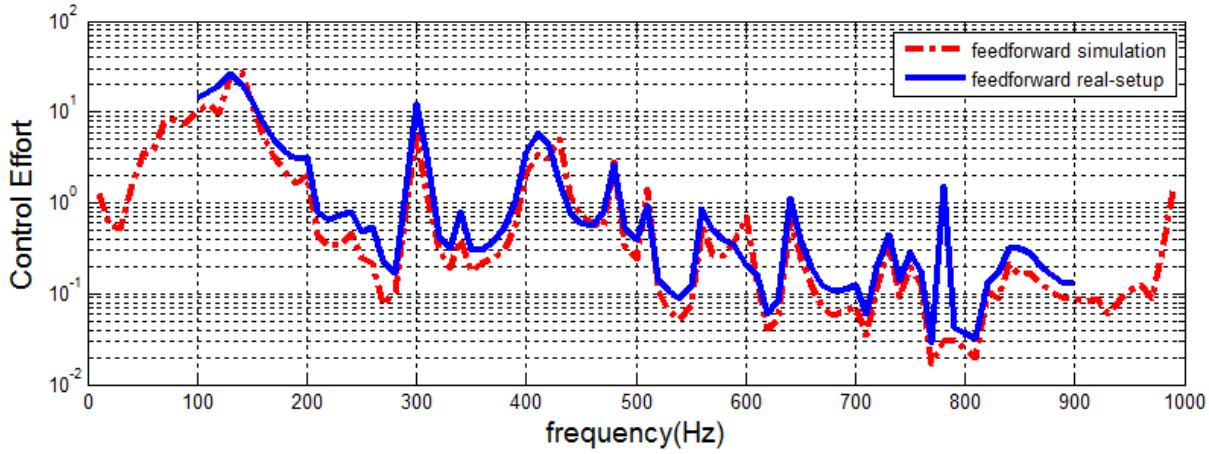

Figure 49 Kinetic energy of the panel in simulation and in the real-setup

In section 4.2.1 it was shown that the adaptation step must at least be 0.4 seconds long. Else a signal is measured that has not reached its steady state yet. However, 0.4 seconds is pretty long and faster adaptation is desirable. Therefore in the following experiment the adaptation step is reduced to 0.2 seconds. In Figure 50 the results of this experiment are compared with the 0.4 seconds adaptation step configuration. For each frequency the steady state is reached after a different waiting time. For frequencies of 310 Hz and 250 Hz this waiting time is the largest. The algorithm will measure wrong phase and amplitude information for these frequencies with the decreased adaptation step time and can not converge to its optimal solution.

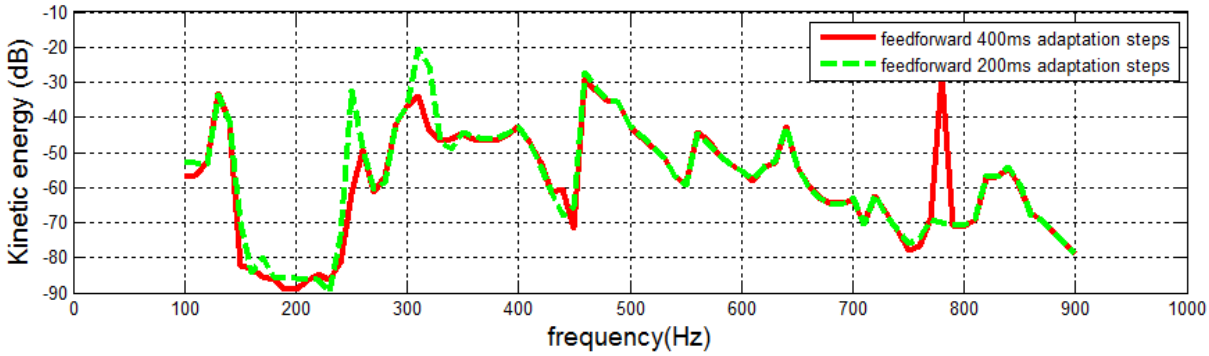

Figure 50 Kinetic energy of the panel for different adaptation rates.

7.7.2 Comparison of different configurations

The configuration of the previous section is compared with two other configurations. The first configuration configures its parameters according to Gersgorin's theorem. The second algorithm uses the actuators on the incident panel and the sensors of the radiant panel. It is a decentralized algorithm, which requires a connection between the two panels. This configuration is not analysed elsewhere in this thesis. However, some experimental tests shown its potential, so this technique is analysed as well. The control effort weighting factors of this configuration are determined with the eigenvalue method.

The results in this section may differ from those in the previous section. Absorbing foam was inserted in the acrylic box which may result in a different frequency response of the system. Also the ventilation in the room in which the experiment was performed was turned off, which lowered the background noise.

The same technique as in the previous section is used here to determine the noise reduction for the entire frequency range. In Figure 51 the kinetic energy of the radiant panel for different control strategies is shown. Both algorithms that use the actuators on the radiant panel can reduce the kinetic energy till approximately 250 Hz. The algorithm based on the eigenvalues of the Hessian matrix performs better. The control strategy that uses the incident panel actuators can reduce the kinetic energy till almost 400 Hz. However, the absolute noise reduction obtained at low frequencies by this algorithm is less.

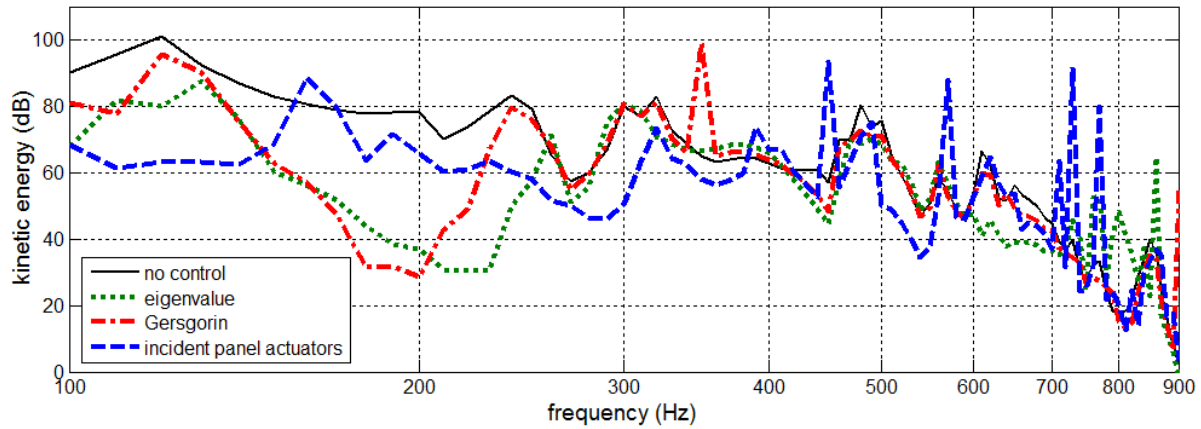

Figure 51 Kinetic energy of the radiant panel for different control strategies.

Furthermore, this control strategy is unstable at several frequencies (for example at 160 Hz). The reason of this unstable behaviour is that the system has not reached its steady state, before its phase and amplitude are measured. The connection between the radiant and incident panel apparently has a larger wait time. In Figure 52 the error signal of a sensor is shown during the adaptation process.

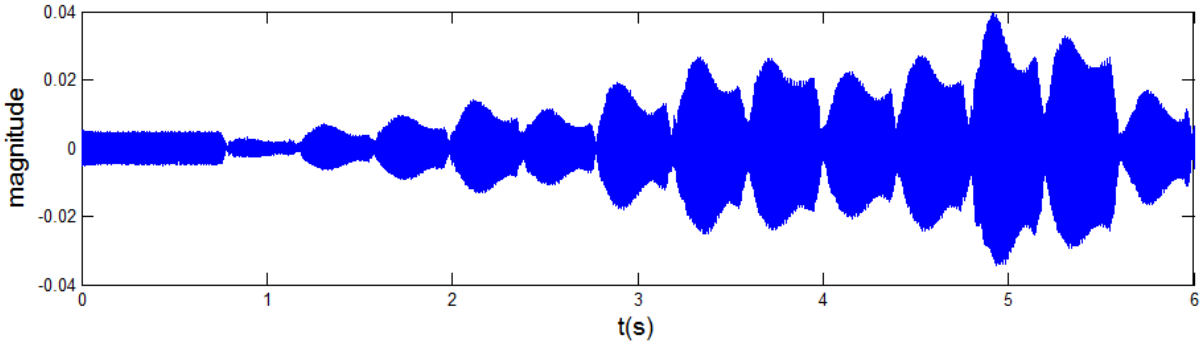

Figure 52 The steady state is not reached after a control signal update. The disturbance signal has a frequency of 160 Hz.

The measured sound pressure level is almost proportional to the kinetic energy of the panel. The sound pressure level is shown in Figure 53. The large reductions of the kinetic energy at 200 Hz of the Gersgorin and eigenvalue method are not proportional. The microphone measures much smaller reductions here.

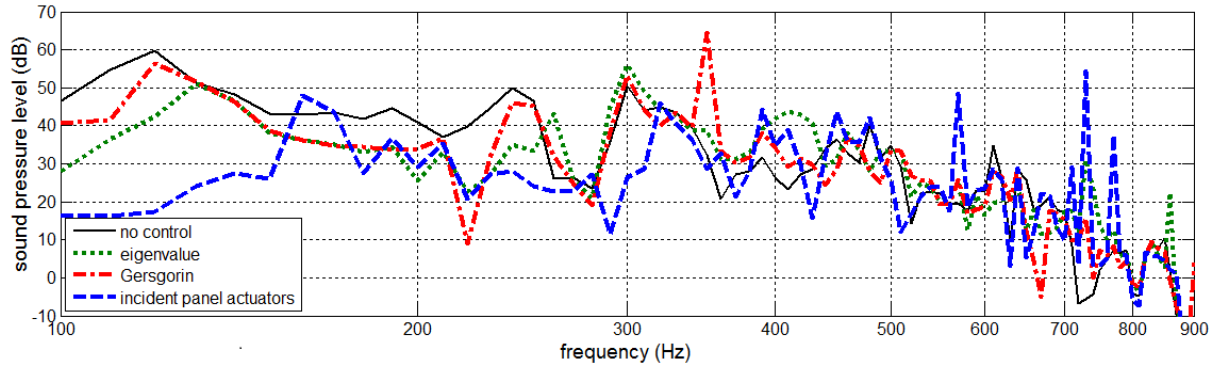

Figure 53 Sound pressure level above the structure for different control strategies.

7.8 Varying disturbance frequency

The blade passage frequency of an airplane is not constant. Dependent on the velocity, the altitude, the acceleration and other factors this frequency may change. In this section the performance of the decentralized harmonic feedforward controller on a frequency changing disturbance signal is analysed. Therefore a disturbance signal that has the following changing frequency is used

$$f_{disturbance} = 200 + 40 \cdot \sin(2\pi f_{control})$$

In this frequency range the controller can achieve a large reduction with a stationary disturbance signal. For three different control frequencies the noise reduction of the feedforward algorithm is

examined. During 90 seconds the sound pressure above the double-structure panel is measured. The first 30 seconds no feedforward control is applied, the next 60 seconds the feedforward controller is activated. In Figure 54, the results of this experiment are shown.

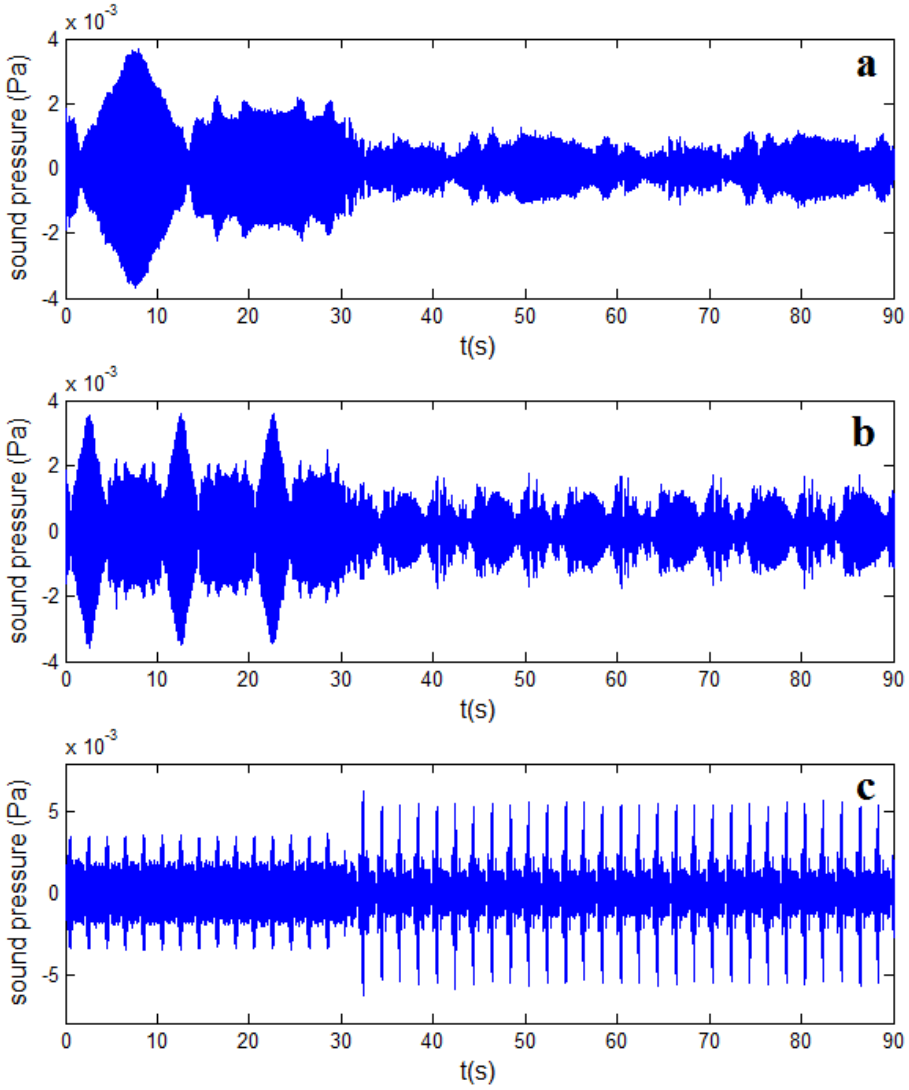

Figure 54 a) $f_{control}$= 1/30Hz, b) $f_{control}$= 1/10Hz, $f_{control}$= 1/2Hz

In this figure, the repeating pattern of the disturbance frequency is clearly visible. The faster the disturbance signal changes the lower the reduction in the measured sound pressure. The performance is quantified by calculating the RMS value of the sound pressure for the both regions. For the control frequency of 1/30 HZ the RMS sound pressure was reduced by a factor 3.18 by the feedforward control. For the other two control signals the RMS sound pressure was reduced by 2.53 and 0.97. Hence, no reduction can be obtained when the frequency changes to fast.

8 Conclusion and recommendations

In this chapter the research questions as described in section 1.3 are answered. Furthermore recommendations are given for further improvement of the harmonic decentralized feedforward controller.

8.1 Conclusion

Examine in simulations if decentralized feedforward control can reduce the sound transmission of the double-panel structure.

With the finite element model of the experimental setup the transfer functions between the different components of the structure are derived. For all frequencies the minimum effort weighting factor of the decentralized controllers is determined. This effort weighting factor is required to make the system stable. If this effort weighting factor is larger than the largest eigenvalue of the plant almost no noise reduction can be obtained. The simulations showed that at almost all frequencies the control effort weighting factor was lower (especially at frequencies below 400 Hz) . Thus, noise reduction is possible with a harmonic decentralized controller.

On both panels sensors and actuators are installed. Which feedforward configuration reduces the sound transmission the most?

The sound transmission is related to the kinetic energy of the radiating panel. To obtain maximum noise reduction the kinetic energy of this panel should be minimised. Experiments have shown that the minimisation of the kinetic energy of the incident panel is not useful. The addition of the extra actuators in this small space makes the system more unstable and larger control effort weighting factors are required. This reduces the overall performance of the system.

Examine the interaction between feedforward and feedback control. Does this combination Improve the robustness of the system?

The addition of feedback control improves the robustness of the system. It reduces the cross-coupling between the decentralized controllers. Thus, smaller effort weighting factors are required, which will result in a larger reduction of the disturbance signal. Feedback control also makes the frequency response of the double-panel structure more flat. This makes it easier to estimate the frequency response; a smaller amount of measurements are required to estimate the entire spectrum accurate.

Select the best feedforward feedback combination

The combination of feedback pressure speakers in the cavity and decentralized feedforward control of the radiant panel reduces the disturbance signal the most in the simulations. In practise this configuration could not be tested, because the pressure speaker feedback controller has not yet been realized.

Find a system identification technique that can initialise the feedforward controllers. This technique should use the components of the feedforward controller as much as possible.

The extra hardware required for analysing and producing the excitation signals must be as little as possible. Hence, the best method is the simple stepped sine excitation signal. All hardware for this method is already present on the decentralized controllers. Multiple frequency components can be transmitted at once. While waiting till the transients of a single frequency disappear, the steady state response of another frequency can be measured.

Is a complete decentralized system possible, that can initialise itself without communicating with a centralized controller?

A decentralized controller has to know the transfer functions from all actuators in the system to its own sensor. With this information a stable decentralized controller can be configured. With Gersgorin's theorem the parameters of the controller are configured. For this process the

decentralized controller has to estimate all the transfer functions. The response of an actuator can be processed locally. However, there has to be a mechanism that tells each decentralized controller when it has to listen and when it has to produce a control signal. Else, all components will talk at the same time and no information of the system is obtained. A decentralized control system that is configured by Gersgorin's theorem can not reduce the sound transmission as much as an optimal algorithm. However, it still can obtain significant reduction at low frequencies.

Implement a decentralized controller and test if noise reduction is possible. Also determine if the simulations agree with the practical measurements
With the system identification system the transfer functions between all components were measured. This data is used in an offline simulation. The observed noise reduction from these models was very similar to the tests on the real-setup. A decentralized feedforward control algorithm can reduce the noise transmission significantly till approximately 250 Hz.

Can the decentralized controller react on a disturbance signal with a varying frequency?
The decentralized controller can react on a varying disturbance signal. Although this signal should not change too fast. The faster the frequency changes the lower the reduction of the disturbance signal.

How much can the disturbance signal be suppressed by the best control strategy?
The sound pressure level above the panel can be reduced by 10 to 20 dB for frequencies below 250 Hz. Above this frequency almost no reduction of the disturbance signal is possible. This reduction is obtained by controlling the radiant panel. The control strategy that uses the actuators on the incident panel and the sensors on the radiant panel can achieve more noise reduction. The sound pressure level above the panel is reduced by 10 to 30 dB for frequencies below 350 Hz. Above this frequency again almost no reduction can be obtained.

8.2 Recommendations

The current system uses the linear least square (LLS) phasor estimator technique to estimate the error signals. This technique should be replaced by the Goertzel algorithm. By replacing this method the computational cost of the decentralized feedforward controller can be reduced significantly. Both techniques can estimate the error signals with the same accuracy.

Feedback control still does not work on the double-panel structure. Also the loudspeaker sources in the cavity of the panel are not yet implemented. Therefore it was not possible to examine the behaviour of the feedforward controller in combinations with the feedback controller. However, in simulations this combination showed significant improvement, so this should be examined in the future.

In this thesis a small experiment on a changing input frequency is performed. However, no real data during a flight of an airplane is used as input to test the controller. This data is required for a real validation of the system.

The feedforward controller can process frequencies parallel as well (similar to the system identification system). A large part of this algorithm is created, however small modifications of this algorithm are required and the system must be tested before it can be used in practise. For optimal

utilisation of the components of a decentralized controller an upgrade to this configuration should be made.

9 Bibliography

1. **Wilby, J. F.** Aircraft interior noise. *Journal of Sound and Vibration.* 190, 1996, pp. 545-564.

2. **Johansson, Sven.** *Active control of propeller-induced noise in aircraft, Algorithms & Methods.* Ronneby, Sweden : s.n., 2000.

3. **Fahy, F and Gardonio, P.** *Sound and structural vibration: radiation, transmission and response 2ed.* London: Academic Press : Elsevier, 2007.

4. **Möser, Michael.** *Engineering acoustics, An introduction to noise control.* Berlin : Springer, 2009.

5. **Pietrzko, Stanislaw J. and Mao, Qibo.** New results in active and passive control of sond transmission through double wall structures. *Aerospace Science and Technology.* 12, 2008, Vol. 2008, pp. 42-53.

6. **Elliott, Stephen J, Stothers, Ian M and Nelson, Philip A.** A multiple error LMS algorithm and its application tot the active control of sound and vibration. 1987, ASSP-35, No 10.

7. **Elliott, Stephen.** *Signal Processing for Active Control.* London : Academic Press, 2001.

8. **Nelson, P.A. and Elliott, S.J.** *Active control of sound.* 1st Edition. London : Academic Press, 1992.

9. *Active control of sound radiation using volume velocity cancellation.* **Johnson, M. E. and Elliot, S. J.** 4, Southamton : Acoustic Society of America, 1995, Vol. 98, pp. 2174-2186.

10. **Guigou, C.** The relationship between volume velocity and far-field radiated pressure of a planar structure. *Journal of sound and vibration.* 197(2), 1996, pp. 252-254.

11. **Fuller, C.R., Hansen, C.H. and Snyder, S.D.** Active control of sound radiation from a vibrating rectangular panel by sound sources and vibration units. *Journal of sound and vibration.* 145(2), 1991, pp. 195-212.

12. **Gardonio, P, Dianchi, E and Elliott, S.J.** Smart panel with multiple decentralized units for the control of sound transmission. Part I: Theoretical predictions. *Journal of sound and Vibration.* Vol 274, 2004, pp. 163-192.

13. **Elliott, Stephen J, Boucher, Christopher C and Nelson, Philip A.** The behavior of a multiple channel active control system. *IEEE Transactions on signal processing.* Vol 40, No 5, 1992.

14. **Bronzel, M.J. and Fuller, C.R.** Implemenation of fast recursive estimation techniques for active control of structural sound radiation. *Active 95; Proceedings of the International Symposium on Active Control of Sound and Vibration.* 1995.

15. **Snyder, Scott D and Tanaka, Nobuo.** Algorithm adaptation rate in active control: Is faster necessarily better. *IEEE transactions on speech and audio processing.* Vol 5, No 4, 1997.

16. *Effect of errors in the plant model on the performance of algorithms for adaptive feedforward control.* **Boucher, C. C., Elliott, S. J. and Nelson, P. A.** 138, Southampton : IEE Proceedings, 1991.

17. *A technique for improved stability of adaptive feedforward controllers without detailed uncertainty measurements.* **Berkhoff, Arthur P.** s.l. : Smart Materials and Strucutres, 2012.

18. **Elliott, Stephen J and Boucher, Christopher C.** Interaction between multiple feedforward control systems. *IEEE transactions on speech and audio processing.* Vol 2, No 4, 1994.

19. **Berkhoff, A.P. and Wesselink, J.M.** Combined MIMO adapative and decentralized controllers for broadband active noise and vibration control. *Mechanical systems and signal processing.* 25, 2011, pp. 1702-1714.

20. **Preumont, A.** *Vibration Control of active structures, An introduction, third edition.* Berlin : Springer, 2011.

21. *A principal component algorithm for feedforward active noise and vibration control.* **Cabell, R. H. and Fuller, C. R.** 227, Hampton : Journal of Sound and Vibration, 1999, pp. 159-181.

22. *Multi-harmonic active structual acoustic control of a helicopter main transmission noise using the principal component analysis.* **Belanger, Pierre, et al.** s.l. : Applied Acoustics, 2009, Vol. 70, pp. 153-164.

23. *Mulit-input multi-ouput feedforward control of multi-harmonic gearbox vibrations using parallel adpative notch filters in the principal component space.* **Pasco, Yann, et al.** Québec : Journal of Sound and Vibration, 2011, Vol. 330, pp. 5230-5244.

24. *Active Vibration Suppression of a Flexible Plate Structure.* **Dong, Zhuomin, Wang, Ying and Bai, Shilei.** harbin : International Conference on Mechatronics and Automation, 2007.

25. *decentralized harmonic control os sound radiation and transmission by a plate using a virtual impedance approach.* **Quaegebeur, Nicolas, Micheau, Philippe and Berry, Alain.** Québec : Acoustic Society of America, 2009. pp. 2978-2986.

26. *Self-tuning control systems of decentralised velocity feedback.* **Zilletti, Michele, Elliot, Stephen J. and Gardonio, Paolo.** Southampton : Journal of Sound and Vibration, 2010, Vol. 329, pp. 2738-2750.

27. *Decentralized control of sound radiation using iterative loop recovery.* **Schiller, Noah H., Cabell, Randolph H. and Fuller, Chris R.** Hampton : Acoustic Society of America, 2010, Vol. 128, pp. 1729-1737.

28. *Decentralized robust vibration control of smart structures with parameter uncertainties.* **Jiang, Jian-Ping and Li, Dong-Xu.** Changsha : Journal of Intelligent Material Systems and Structures, 2011, Vol. 22.

29. *Experimental implementation of a self-tuning control system for decentralised velocity feedback.* **Zilletti, Michele, et al.** Southampton : Journal of Sound and Vibration, 2011, Vol. 331.

30. *Fundamentals of noise and vibration.* **Fahy, Frank and Walker, John.** London : Routledge, 1998.

31. Particle velocity. *Wikipedia.* [Online] 2012. [Cited: 3 July 2012.] http://en.wikipedia.org/wiki/Particle_velocity.

32. Complex multiplication. *Wolfram MathWorld.* [Online] http://mathworld.wolfram.com/ComplexMultiplication.html.

33. *On Linear least squares approach for phase estimation of real sinusoidal signals.* **So, Hing-Cheung.** 88, s.l. : IEICE Trans. Fundamentals, 2005.

34. **Pintelon, Rik and Schoukens, Johan.** *System Identification A frequecny domain approach.* New york : IEEE Press, 2001.

35. *Panel Resonance Control and Cavity Control in Double-Panel Structures for Active Noise Reduction.* **Ho, Jen-Hsuan and Berkhoff, Arthur.** Enschede : International Conference on Adaptive Structures and Technologies, 2011.

36. **Douglas, Scott C.** Fast implementations of the filtered-X LMS and LMS alforithms for multichannel active noise control. *IEEE transactions on speech and audio processing.* Vol 7, No4, 1999.

37. **Tao, Tao and Frampton, Kenneth D.** Experiments on distributed active vibration control of a simply supported beam. *Smart material structures.* 15, 2006, pp. 1858-1862.